NASA Contractor Report 195429

Prediction of Wind Tunnel Effects on the Installed F/A-18A Inlet Flow Field at High Angles-of-Attack

Crawford F. Smith
NYMA, Inc.
Engineering Services Division
Brook Park, Ohio

January 1995

Prepared for
Lewis Research Center
Under Contract NAS3–27186

National Aeronautics and
Space Administration

Prediction of Wind Tunnel Effects on the Installed F/A-18A Inlet Flow Field at High Angles-of-Attack

NASA CR

C. F. Smith
NYMA, Inc.
Engineering Services Division
Brook Park, Ohio 44142

TABLE OF CONTENTS

LIST OF TABLES

LIST OF FIGURES

Nomenclature

B	Wind tunnel width
C_p	$(P - P_\infty)/(0.5\ \rho_\infty\ V_\infty^2)$
Corrected Flow Rate	$(\dot{m}\ \sqrt{\theta})/\delta$
Distortion	$(PT_{max} - PT_{min})/PT_{avg}$ at compressor face
FS	Fuselage Station in full scale inches (FS = 0 located 60.5 inches ahead of nose)
$\dot{m}$	Mass flow rate
P	Local static pressure
P_∞	Free-stream static pressure
P_T	Local total pressure
$P_{T_{avg}}$	Average total pressure (based on 40 probe rake at compressor face)
P_{T_∞}	Free steam total pressure
$P_{T_{min}}$	Minimum total pressure
$P_{T_{max}}$	Maximum total pressure
Recovery	Average ratio of P_T/P_{T_∞} from 40 probe rake
X	Wind tunnel axial distance
$T_{T_{avg}}$	Average total temperature
V_∞	Free stream velocity
α	Angle-of-Attack
β	Angle-of-Yaw
δ	$P_{T_{avg}}/(14.696 lb/in^2)$
ρ_∞	Free-stream density
θ	$T_{T_{avg}}/519.0°R$ at compressor face

Summary

NASA Lewis is currently engaged in a research effort as a team member of the High Alpha Technology Program (HATP) within NASA. This program utilizes a specially equipped F/A-18A, the High Alpha Research Vehicle (HARV), in an ambitious effort to improve the maneuverability of high-performance military aircraft at low-subsonic-speed, high angle-of-attack conditions. The overall objective of the Lewis effort is to develop inlet technology that will ensure efficient airflow delivery to the engine during these maneuvers. One part of the Lewis approach utilizes computational fluid dynamics codes to predict the installed performance of inlets for these highly maneuverable aircraft.

Wind tunnel tests were a major component of the Lewis program. Since the available wind tunnel was small (9 × 15 ft) as compared to the scale of the model of the F/A-18A (19.78%), there were questions about the capability to obtain useful inlet performance data. The blockage effects were expected to be very large. This report represents the results of an analysis to determine how the wind tunnel walls affect inlet performance at several angles-of-attack.

The predictions for the external particle traces along the fuselage indicate the influence of the wind tunnel side wall under the model is greater at 30° angle-of-attack than at 50° angle-of-attack on the under Leading Edge Extension (LEX) vortex trajectory. The side wall above the model appears to have negligible influence on the under LEX vortex. This may be due to the LEX

acting as "shield" to the upper wall effects. As expected, the wind tunnel has a significant influence on the external forces. The lift and drag coefficients increase significantly for the wind tunnel model as compared to free stream conditions.

The wind tunnel had a small effect on the inlet recovery and on inlet total pressure distortion patterns. The predicted recoveries for the wind tunnel model are within one percentage point of the model recoveries in free stream conditions.

1.0 Introduction

NASA Lewis is currently engaged in a research effort as a team member of the High Alpha Technology Program (HATP) within NASA. This program utilizes a specially equipped F/A-18A, the High Alpha Research Vehicle (HARV), in an ambitious effort to improve the maneuverability of high-performance military aircraft at low-subsonic-speed, high angle-of-attack conditions. The overall objective of the Lewis effort is to develop inlet technology that will ensure efficient airflow delivery to the engine during these maneuvers. One part of the Lewis approach uses computational fluid dynamics codes to predict the installed performance of inlets for these highly maneuverable aircraft.

One of the goals of the (HATP) is to predict accurately the aerodynamics of aircraft operating at extreme attitudes (α=60°, β= 10°). As part of this program, NASA Ames-Dryden, Ames-Moffett and Langley are concentrating on external aerodynamics, including thrust vectoring control systems and vortex flow control. NASA Lewis is studying the effects of high angle-of-attack and yaw flight conditions on flow within the F/A-18A inlet duct. Details of this cooperative program are contained in Ref. 1.

The F/A-18A aircraft has experienced engine stalls at high angles-of-attack and yaw flight conditions that were outside of the flight envelope. At these flight conditions, high angular rates were also present. Future fighter aircraft will be designed to operate routinely in this flight regime. Therefore, essential understanding of the inlet flow field at these flight conditions should be obtained. Due to the complex interactions of the fuselage flow field and the inlet flow field,

a study of the flow within the inlet must also include the external effects. Past calculations of flow about the F/A-18A have not included the inlet and ramp [Ref. 2,3]. These features are usually fared over and assumed not to influence the external flow field significantly. However, the effects from the upstream forebody, LEX and diverter must be included in order to provide the proper inflow conditions to the inlet duct. The results of including the inlet and ramp in the flow simulation are reported in Ref. 4. The solutions obtained in this previous study were evaluated, and several short-comings were identified. This resulted in obtaining a much more detailed and complete geometry data base of the F/A-18A aircraft and inlet. In addition several areas of the computational grid were revised to improve flow field and surface resolution. Although the grid was refined, the total number of grid points used to model additional components in the revised grid increased only approximately 10%. This was accomplished by reducing the number of grid points in regions where the flow field did not appear to have a significant impact on the inlet flow conditions. The results of this study are reported in Reference 5.

A major concern in conducting the wind tunnel tests was the effects of the wind tunnel wall on the inlet flow field due to blockage effects. The 9×15 wind tunnel [Ref. 6] is considered small for testing a 19.78% scale model of the F/A-18A aircraft. Although the tunnel is too small for external flow testing, the effects of the tunnel walls on the inlet performance was not known. Previously cited references concerning the calculations of the F/A-18A inlet performance had discrepancies with data reported in those references. However, the pre-

dicted *changes* from free-steam performance due to wind tunnel walls should be reasonably valid. Past experience has demonstrated that the calculations are reliable for predicting flow *changes* due to geometric or upstream flow condition changes, though the absolute values of performance may not be accurate [Ref. 4]. Therefore, this report presents the results of an analysis to determine how the wind tunnel walls affect inlet performance by comparing free-stream calculations to calculations obtained in the wind tunnel for 30° and 50° angle-of-attack. For each angle-of-attack, two free-stream Mach numbers: 0.2 and 0.15, were employed. These conditions reflect those that would occur in the tunnel.

This report has four sections: Section 2.0 covers the wind tunnel tests; Section 3.0 discusses the numerical modeling; Section 4.0 the results and Section 5.0, major conclusions and recommendations.

2.0 Experimental Program

An experimental program to study the inlet duct flow was planned at Lewis. The wind tunnel tests were canceled due to budgetary considerations and shifts in program priorities. For completeness and future reference, an overview of the test program is included. A 19.78% scale forebody/inlet model of the F/A-18A aircraft would have been tested in the Lewis 9×15 wind tunnel. Details of the airframe aft of the engine face plane were not included. Planned measurements include steady and dynamic total pressure surveys at various stations within the inlet, and a 40 probe total pressure rake at the compressor face, a flow angle survey at the inlet entrance, surface static pressure measurements along the forebody and inlet walls and laser light sheet flow visualization of the flow ahead of the inlet. The effects of free stream Mach number, mass flow rate, angle-of-attack and yaw would be investigated.

3.0 Numerical Modeling

This section presents: 1) the major features of the NPARC3D code including boundary conditions; and 2) a brief discussion of the computational grid.

3.1 NPARC3D Code

The NPARC3D code, Version 1.0 [Ref. 7] solves the full three-dimensional Reynolds averaged Navier-Stokes equations in strong conservation form using the Beam and Warming approximate factorization scheme to obtain a block tridiagonal system of equations. Pulliam's scalar pentadiagonal transformation provides an efficient solver. The code uses the Baldwin-Lomax turbulence model [Ref. 8]. Specifically, the NASA Lewis version of this turbulence model does not use the streamwise component of vorticity to determine the turbulent viscosity [Ref. 9]. This approach improves the modeling of vortical flows in ducts. The implicit scheme uses artificial dissipation to eliminate oscillations in the solution caused by the use of central differences. This code also uses multiple grid blocks. Trilinear interpolation [Ref. 10] transfers information at the grid block interfaces.

3.2 Grid Generation

Accurate modeling of the geometry and judicious clustering of grid points are needed for a correct numerical solution and an economical computation. The complex multi-block grid used for these calculations, which was very effective, was created with the GRIDGEN Version 6.0 grid generation system [Ref. 12].

McDonnell-Douglas supplied the geometry database used for the grid: x, y, z coordinate points given at axial cuts along the fuselage. The database

defined the fuselage, LEX, wing, tail, ramp , LEX slot, diverter, inlet highlight and the inlet. The geometry is shown in Figure 1.

Complex interactions between the fuselage flow field and the inlet flow field, required the inclusion of the forebody, fuselage, LEX, ramp and wing in the grid. The horizontal tail, vertical tail, aft fuselage and the nozzle were not modeled because they have minimal effects on the inlet flow field. The wing leading edge flap, which is deflected down 34° when the aircraft is at 30° angle-of-attack, is included. An embedded c-grid about the inlet highlight is also included to improve the resolution of flow gradients and surface geometry. A pair of vortex generators which are positioned approximately halfway downstream in the inlet were not modeled due to their small size.

Having discussed the components of the aircraft included in the computational model, details of the grid are presented. The overall grid block structure is shown in Figure 2 for the free-stream model. The free stream model consists of 23 blocks. The plane of symmetry and surface grids are shown in Figure 3. The grid consists of approximately 1.2 million points. The forebody, underlex and inlet duct grids were used to compute the viscous flow with a grid spacing of y+ of approximately 1 off the surface. The grids above the LEX and along the fuselage aft of the inlet were used to calculate inviscid flow and were much coarser. The viscous effects were deemed significant for the inlet performance calculations ahead of the inlet and under the LEX.

The overall block structure of the model in the 9×15 wind tunnel for 30° and 50° angle-of-attack are shown in Figures 4a and 4b, respectively. The grids for

these two cases are shown in Figures 5a and 5b. The wind tunnel was modeled for inviscid flow without the slots that are present in the actual wind tunnel. This approach to modeling the wind tunnel walls provides a worst-case scenario for the wind tunnel blockage effects on the inlet performance. If the performance is close to free stream predictions, including the slots will only improve the calculations. They will not be necessary though, unless, significant differences occur between the free stream performance predictions and the wind tunnel simulations. Since the model is situated far downstream of the tunnel inlet, we chose not to model the tunnel inlet section. Also, from previous free stream calculations we knew that the downstream external flow boundaries do not affect the aircraft inlet flow field significantly. The downstream tunnel diffuser was also not included in the simulation. If the tunnel simulation of the inlet flow field results differ significantly from the free stream results, these assumptions would be reevaluated and additional tunnel modeling may be performed.

3.3 Boundary Conditions

Total conditions were specified at the wind tunnel test section entrance, and static conditions were specified at the exit. The downstream static pressure was adjusted to obtain the desired upstream Mach number. The wind tunnel walls were modeled as solid, slip surfaces with no bleed, although the actual walls contained slots. For the free stream calculations, farfield type boundary conditions were imposed along the outer computational boundaries. This condition uses a one-dimensional Riemann invariant to maintain the free-stream flow conditions. Along the windward side of the airframe, no-slip, adiabatic

conditions were specified. Along the leeward side of the aircraft, inviscid flow is specified. The static pressure at the inlet duct exit was adjusted to obtain the equivalent experimental corrected mass flow rate: based upon total pressure at the engine face plane that was obtained from an average of 40 total pressures in a configuration of 8 equally spaced legs, with 5 equal area total pressure locations per leg. Symmetry conditions were assumed along the centerline of the aircraft. Trilinear interpolation transfers data between the grid blocks.

4.0 Results

4.1 External Flow Field

In this section, the significant external flow features are discussed. The first section discusses the general features of the vortical flows present along the F/A-18A fuselage at high angles-of-attack. Details of the flow field near the inlet entrance (along the ramp) are then examined to indicate the influence of the wind tunnel walls on the near-inlet flow field. These flow features are examined as a function of angle-of-attack and as a function of free-stream Mach number. The angle-of-attack will influence the amount of blockage in the wind tunnel. The free-steam Mach number affects the inlet capture streamtube area. The examination of the flow field from the aircraft nose to the inlet entrance reveals how influential the wind tunnel walls are on the local external flow as one proceeds from the nose to the inlet. The graphical results in this report were obtained from the PLOT3D code [Ref. 13]. The section concludes with a discussion of static pressure distributions on the model and wind tunnel walls.

Flow Along Fuselage

At 30° angle-of-attack, a vortex forms under the LEX (see Figure 6). In addition, another vortex forms along the aircraft's leeward side originating at the apex of the LEX-fuselage intersection. The windward vortex develops when the flow impinges on the bottom of the LEX and moves down the fuselage until it separates from the surface.

Having discussed the general three-dimensional features of the external flow, the details of the surface flow along the fuselage are presented. Surface parti-

cle traces for 30° angle-of-attack are shown in Figure 7a. For Mach 0.2, both traces indicate two separation lines. An examination of cross stream vector plots indicate that: 1) a small secondary vortex embedded under the primary LEX vortex and that 2) the circumferential grid resolution is not sufficient to resolve the separation lines attributed to this secondary vortex. At this angle-of-attack, the wind tunnel model appears to offer a straighter trajectory of the under-LEX vortex traces than the free stream model. This may be caused by the side wall, along the underside of the model, influencing the flow field.

For Mach 0.15, the traces for both cases indicate a single line of separation. From another examination of the cross stream velocity vectors, the secondary vortex disappears. This secondary vortex appears to be caused by a Reynolds number related phenomena. The Mach 0.2 case shows that the wind tunnel traces move upward toward the LEX more than the free stream case.

Figure 7b shifts from surface particles at 30° angle-of-attack to 50° angle-of-attack. For the Mach 0.2 case, few differences develop between the free stream and wind tunnel model traces. The side wall under the model is much farther away than the 30° angle-of-attack case and appears to have very little influence on the flow field under the LEX. Although the side wall above the LEX is very close to the wind tunnel model, the LEX itself "shields" the under LEX flow field from the wall and therefore has a negligible influence on the flow under the LEX. For this angle-of-attack, only a single vortex is apparent under the LEX. For Mach 0.15, the particle traces are very similar to those obtained at Mach 0.2.

Flow Along Ramp

Figure 8a moves the focus from the fuselage surface to the ramp at 30° angle-of-attack. For Mach 0.2, the free stream and tunnel model traces are very similar, a result that holds for the Mach 0.15 case. The inlet flow appears to dominate the external flow field along the ramp with negligible influence from the wind tunnel.

Figure 8b, moves to 50° angle-of-attack, where striking similarities develop: traces for the free stream and wind tunnel cases are very similar at all Mach numbers and angles-of-attack. This similarity for significantly different angles-of-attack supports the premise that the inlet flow is dominating the external flow along the ramp.

Static Pressure Distributions on Model and Tunnel Walls

Another way of quantifying the wind tunnel wall effects on the external flow field is to examine the change in surface static pressure distributions from free stream conditions. Surface static pressure measurements from a flight test were made at several fuselage locations [Ref. 14] as shown in Figure 9. A previous fully turbulent numerical study [Ref. 4] indicated that the effects of 19.78% scale were negligible for this type of data and that full scale data could be compared with these subscale results. Free stream data for 30° angle-of-attack are compared to numerical results in Figure 10a. Data are not available for 50° angle-of-attack. The free stream numerical results for the surface static pressures along the forebody and LEX agree with the data [Ref. 14], as shown in Figure 10a. The discrepancies between the numerical results and the data along

the forebody may be due to the lack of adequate grid resolution of the vortex-dominated region of the flow. Another source for the discrepancies may be laminar-to-turbulent transitioning flow, which is present in the full scale vehicle [Ref. 14] and not modeled in the calculations. Along the top side of the LEX the agreement is poor due to lack of grid resolution and the use of the inviscid flow approximation in this region (hence, no comparison).

The effects of the wind tunnel are shown in the 30° angle-of-attack results shown in Figure 10a. At Mach 0.2, the wind tunnel model static pressure distributions indicate a more negative static pressure coefficient than in the free stream computations. In Figures 10b, the wind tunnel model shows a similar trend for Mach 0.15 results. A similar set of results is evident for 50° angle-of-attack as shown in Figures 10c and 10d. The changes in pressure along the forebody and LEX are apparently a tunnel-blockage effect. The surface pressure coefficients are not affected by upstream Mach number in the free stream cases: the static pressure coefficient distributions are identical for both free stream Mach numbers. The exception is for 50° angle-of-attack with a free stream Mach number of 0.2. A small degree of oscillation was observed in the static pressures as the solution iterated. This may be due to some instability in the top LEX vortex that the coarse grid is not capturing effectively. The top side of the LEX is much more sensitive to tunnel walls than the underside of the LEX, as angle-of-attack is changed.

When we examine wind tunnel effects, we can check the static pressures along the walls for solid blockage and wake blockage effects [Ref. 15, 16]. Figure

11 displays the surface static pressure coefficients along the centerlines of the top, bottom and side walls of the tunnel. The top side corresponds to the model canopy side wall, the bottom corresponds to the lower fuselage side wall and the side corresponds to the wall (tunnel ceiling) near the wing tip. One observation that can be made from these pressure distributions is the downstream boundary is too close to the model to allow the static pressure coefficient to reach an asymptotic value. However, it appears the downstream asymptotic value will be a significant non-zero value.

For 50° angle-of-attack, this value will be much more negative than the 30° value. These non-zero downstream pressure coefficients indicate the level of wake blockage present in the tunnel which increases as the angle-of-attack increases. For a given angle-of-attack, the levels appear to be insensitive to the upstream Mach number. The effects of solid and wake blockage on drag can be obtained using the pressure distributions as input to a method of images approach described in Reference 15. Since this analysis used many approximations, the effects of solid and wake blockage were not quantified. Similar observations can be made from the tunnel wall static-to-total pressure distributions shown in Figure 12.

4.2 Inlet Duct Flow Field

This section, examines two aspects of the inlet duct flow field: 1) predicted total pressure contours at the inlet entrance and exit; 2) predicted exit total pressures contours are compared with experimental total pressure contours for 30° angle-of-attack and free-stream Mach Number of 0.2.

Total Pressure Contours

The inlet entrance total pressure contours for 30° angle-of-attack are shown in Figure 13a and for 50° angle-of-attack in Figure 13b – as well as free stream Mach numbers of 0.2 and 0.15. For all cases, the wind tunnel results indicate a slightly larger region of cross-stream separation along the inside of the outboard lip. The size of the separation is larger for Mach 0.15 than Mach 0.20 free stream flow. As the Mach number increases, the capture streamtube stagnation point moves from the outside of the lip toward the highlight, thus reducing the magnitude of the cross-stream separation. From previous calculations, not presented in this report, the cross-stream separation is not present for free-stream Mach numbers greater than 0.4. At this condition, the stagnation point of the capture streamtube moves inside the lip. From a review of animated results using the FAST program [Ref. 17], this cross-stream separation region migrates towards the bottom of the duct as it moves downstream and is a significant contributor to the total pressure distortions calculated at the compressor face.

Figure 14a shifts the focus from the inlet entrance to the compressor face. The inlet compressor face total pressure contours are shown in Figure 14a for 30° angle-of-attack and in Figure 14b for 50° angle-of-attack: results for upstream Mach numbers of 0.2 and 0.15 are shown. The effect of the wind tunnel is to slightly increase the size of the low total pressure region as compared to the corresponding free stream case. Although the external flow field was affected significantly, the inlet flow field appears relatively insensitive to the tunnel walls.

Inlet Recovery and Distortion

A comparison of the predicted inlet recoveries and distortions for both Mach numbers and angles-of-attack are shown in Table 1. The wind tunnel effect on recovery appears to be small for all cases. The change in predicted recovery is one-half percentage point for Mach 0.2 and one percentage point for Mach 0.15 upstream flows. For distortion, the change in Mach number appears to be more significant at 30° angle-of-attack than for 50° angle-of-attack. This may be due to the significant amount of distortion at 50° angle-of-attack overwhelming the added effects of the wind tunnel. In addition, the effect of the wind tunnel on the inlet distortion values were much greater for the upstream Mach number of 0.15 than 0.20.

For the Mach 0.2, 30° angle-of-attack case, there data is available from a 19.2% scale model test [Ref. 18]. Figure 15 compares the computed free stream case with time-averaged data and instantaneous data which reveals significant discrepancies. This indicates that the flow is very unsteady. The NPARC3D results compare more favorably with the instantaneous data than the time averaged data. To simulate the time-averaged data, we need 1) a time accurate solution and 2) the average of the total pressure results obtained at the compressor face for a suitable number of time steps. From previous experiments, we know that these distortion patterns move in space and vary in strength with time, so the time-averaged distortion pattern represents a "smeared" contour pattern. The NPARC solution represents a steady state or asymptotic numerical solution and does not capture the unsteady nature of the flow field. However,

the general distortion pattern does resemble the experimental pattern indicating that the code has captured a significant amount of the overall physics (see Reference 12). The objective of this investigation is the *changes* predicted in inlet performance due to the wind tunnel and not the *absolute* levels of performance. From this perspective, the predictions should be reliable.

4.3 Numerical Issues

For such a complex problem, determining convergence is not a straightforward task. Residuals are not very reliable since they tend to drop only three orders of magnitude for complex viscous flows. Therefore, we follow the flow quantities of interest as the solution iterates to determine when these quantities stop changing or the changes per iteration become minimal.

Several quantities are presented for convergence criteria in the following discussion. The calculated forces on the aircraft served as one measure of convergence of the external flow field. The predicted lift and drag coefficients for the free stream cases varied by less than one percent as the solution iterated. For the wind tunnel cases, the variation in lift and drag coefficients was less than one-half percent. The exception was for both free stream and wind tunnel cases at 50° angle-of-attack and an upstream Mach number of 0.2 where the lift and drag coefficients varied by 2 percent. From examining the surface static pressure diagrams as the solution iterated, not shown in this report, it appears the pressures along the upper LEX exhibit a larger oscillation as the solution iterates for Mach 0.2 and 50° angle-of-attack than for the other cases. This may be due to some instability in the top LEX vortex that the coarse grid is not

capturing effectively.

For the inlet duct flow, a measure of convergence is the inlet mass flow rate changes as the solution iterated. All solutions obtained compressor face corrected mass flow rates that varied by one percent or less as the solution iterated. The maximum change in the flow rate at any computational station within the inlet duct from the inlet entrance flow rate was 1.5 percent.

5.0 Conclusions and Recommendations

The external flow calculations revealed that the tunnel walls had a significant influence on the external flow field. The surface static pressure distributions along the fuselage and LEX changed significantly from the free stream cases when the model was simulated in the tunnel. Similarly, the lift and drag coefficients increased significantly from the corresponding free stream cases.

The actual inlet flow for the conditions examined was very unsteady. A time accurate solution may be required to simulate the time averaged total pressure contours presented in the experimental results. However, previous studies indicate that the simulation has captured the major flow phenomena. Although the absolute values of some computational results may differ from data, the effects of changes in free stream conditions, such as the inclusion of the tunnel walls can be reliably predicted.

Although the tunnel walls significantly affected the external flow field, inlet duct performance was much less affected. The inlet recovery for the wind tunnel model decreased less than one percentage point from the recoveries predicted for free stream conditions. The inlet total pressure distortions at the compressor face increased up to three percentage points from similar free stream conditions. The effects of the tunnel were more pronounced as the upstream Mach number decreased.

From the results obtained in this study it appears that although wind tunnel blockage effects are significant on the external flow field , useful inlet performance data can be obtained that can then be related back to flight data.

6.0 Acknowledgements

Support of this work by the NASA Lewis Research Center of the National Aeronautics and Space Administration under contract NAS3-27186 is gratefully acknowledged. Interest shown by NASA Project Manager, Thomas Biesiadny, is particularly appreciated. Jim Bruns and Steve Podleski provided excellent grid generation work. While Raymond Cosner of McDonnell-Douglas Company supplied the F/A-18A airframe geometry database. In addition, the author thanks Tammy Langhals for her outstanding work in generating the figures and text.

7.0 References

1. Aeropropulsion '91, NASA CP 10063, Proceedings of a conference held at NASA Lewis Research Center, Cleveland, Ohio, March 20-12, 1991.
2. Ghaffari, F., Bates, B.L., Luckring, J.M., Thomas, J.L., and Biedron, R.T., "Navier-Stokes Solutions about the F/A-18 Wing-LEX-Fuselage Configuration with Multi-Block Structured Grids", AIAA Paper No. 91-3291, Presented at the 9th Applied Aerodynamics Conference, Baltimore, Maryland, September 23-25, 1991.
3. Gee, K., Tavella, D., and Schiff, L.B., "Computational Optimization of a Pneumatic Fuselage Forebody Flow Control Concept", AIAA Paper No. 91-3249, Presented at the 9th Applied Aerodynamics Conference, Baltimore, Maryland, September 23-25, 1991.
4. Bruns, J.E. and Smith, C.F., "Full Navier-Stokes Calculations on the Installed F/A-18 Inlet at a High Angle-of-Attack", AIAA Paper No. 92-3175, Presented at the AIAA/SAE/ASME/ASEE 28th Joint Propulsion Conference and Exhibit, Nashville, Tennessee, July 6-8, 1992.
5. Smith, C.F. and Podleski, S.D., "Installed F/A-18 Inlet Flow Calculations at 30 Degrees Angle-of-Attack: A Comparative Study", AIAA Paper 94-3213, Presented at the 30th Joint Propulsion Conference, Indianapolis, Indiana, June 27-29, 1994.
6. Yuska, J.A. and Diedrich, J.H., "Lewis 9- BY 15- Foot V/STOL Wind Tunnel", NASA TM X-2305, July 1971.
7. Cooper, G.K. and Sirbough, J., "The PARC Distinction: A Practical Flow Solver", AIAA Paper No. 90-2002, July 1990.
8. Baldwin. B.S. and Lomax, H., "Thin Layer Approximation and Algebraic Turbulence Model for Separated Turbulent Flows", AIAA Paper No. 78-257, Jan. 1978.
9. Sirbaugh, J.R., and Reichart, B.A., "Computation of a Circular-to-Rectangular Transition Duct Flow Field", AIAA Paper No. 91-1741, Presented at the 22nd Fluid Dynamics, Plasma Dynamics and Lasers Conference, June 24-26, 1991, Honolulu, Hawaii.
10. Stokes, M.L. and Kneile, K.L., "A Search/Interpolation Algorithm for CFD Analysis", Presented at the World Congress on Computational Mechanics, University of Texas, Austin, Texas, September 1986.
11. Steinbrenner, J. P., Chawner, J. R., and Fouts, C. L., "The Gridgen 3-D Multiple Block Grid Generation System," WRDC-TR-90-30222, 1991.
12. Smith, C.F. and Podleski, S.D., "Installed F/A-18 Inlet Flow Calculations at 30 Degrees Angle-of-Attack: A Comparative Study", NASA CR 195297, April 1994. This reference contains much more detail than Ref. 5.

13. Walatka, P.P., Buning, P.G., Pierce, L. and Elson, P.A., "PLOT3D User's Guide", NASA TM 101067, March 1990.

14. Fisher, D. F., Banks, D. W., Richwine, D. M., "F-18 High Alpha Research Vehicle Surface Pressures: Initial In-Flight Results and Correlation with Flow Visualization and Wind-Tunnel Data," NASA TM 101724, 1990.

15. Hackett, J.E. and Wilsden, D.J., "Determination of Low Speed Wake Blockage Corrections via Tunnel Wall Static Pressure Measurements", AGARD-CP-174, Wind Tunnel Design and Testing Techniques, October 1975.

16. Rae, R.H. and Pope, A., "Low-Speed wind Tunnel Testing", ISBN 0-471-87402-7, John Wiley and Sons, 1984.

17. Walatka, P.P., Plessel, T., McCabe, R.K., Clucas, J., Elson, P.A., "FAST User's Manual", NASA Ames Research Center: WAO and RND, Beta 2.0, RND-91-011, December 1991.

18. Amin, N.F., Hollweger, D.J., Franks, W.J., de la Vega, E.G., Yamada, M., and Tsukahira, T.W., "AEDC Series 1 F-18, .192 Scale Inlet Analysis Report", NOR 77-310, Northrop Corporation, Aircraft Division, Hawthorne, California, May 1977.

Table 1. Predicted Inlet Performance Summary

	Corrected Flow (lbm/sec)	Recovery (%)	Distortion (%)
$M_\infty = 0.2, \alpha = 30°$			
Model	144.4	92.9	23.5
Tunnel	142.9	92.3	24.1
$M_\infty = 0.15, \alpha = 30°$			
Model	146.7	91.5	24.4
Tunnel	145.7	90.6	27.2
$M_\infty = 0.2, \alpha = 50°$			
Model	144.9	88.9	30.9
Tunnel	144.2	88.3	30.8
$M_\infty = 0.15, \alpha = 50°$			
Model	143.9	89.2	30.2
Tunnel	144.4	88.2	31.9

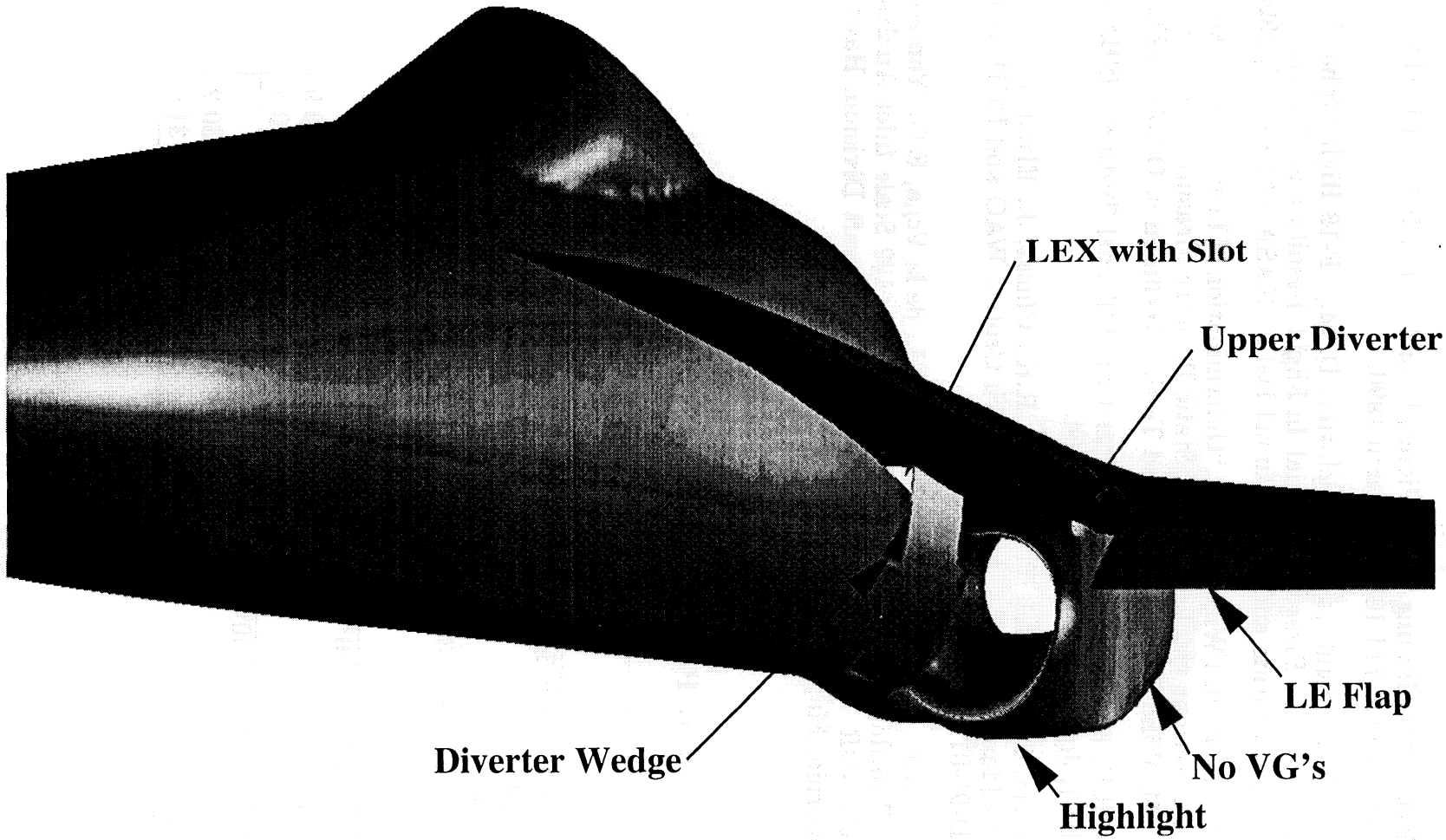

Fig. 1 – F/A–18A Geometry

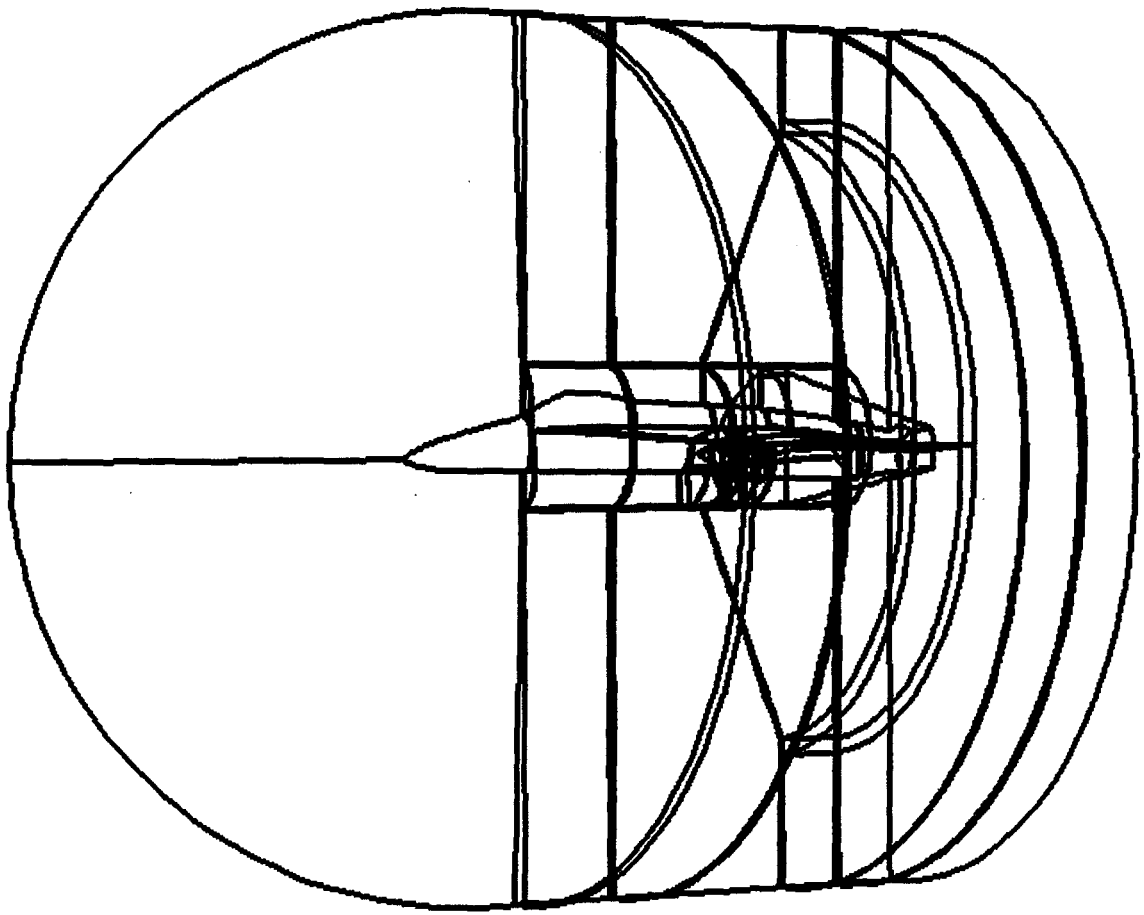

Fig. 2 – F/A–18A Grid Block Structure

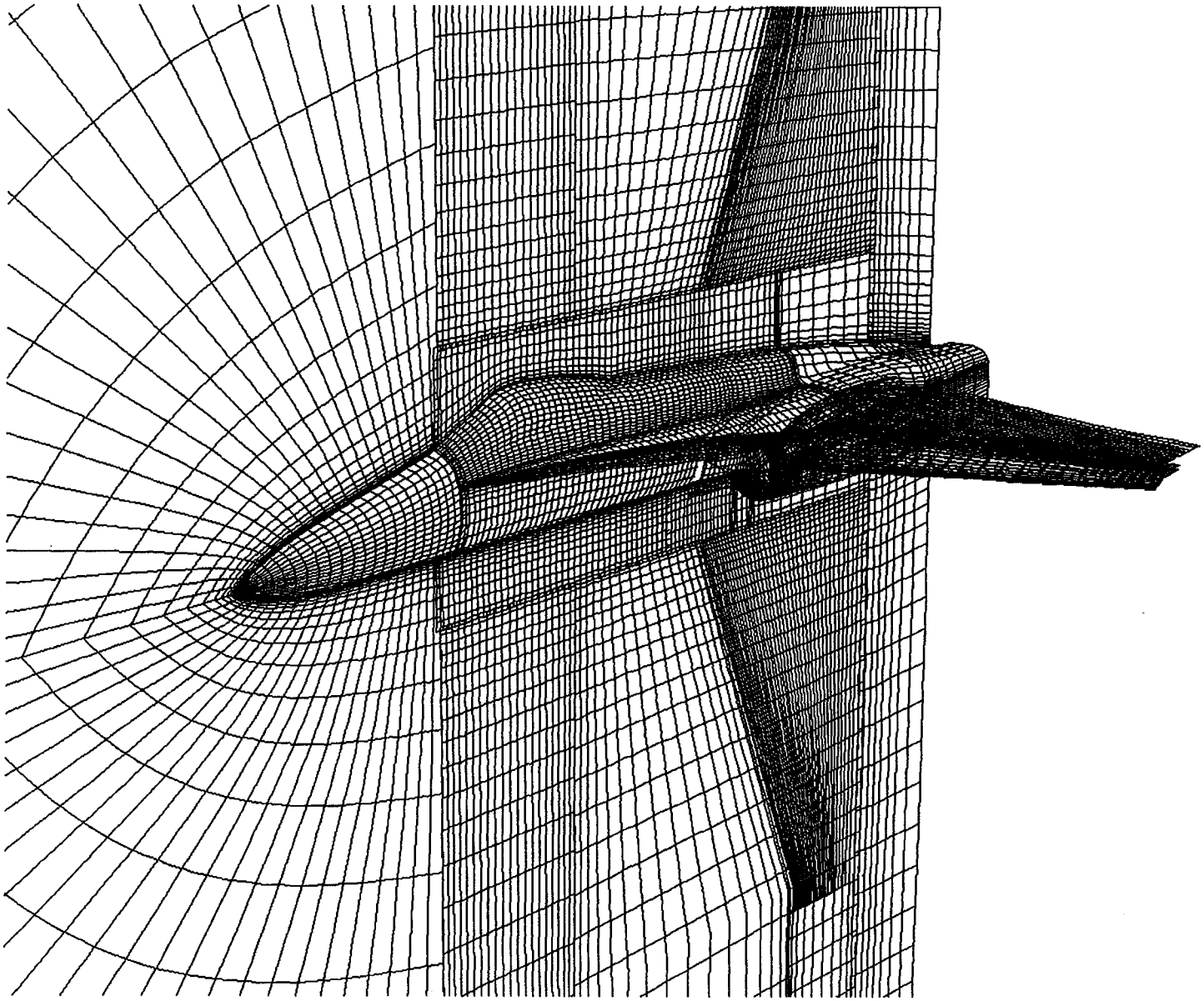

Fig. 3 – F/A – 18A Surface and Plane of Symmetry Grid

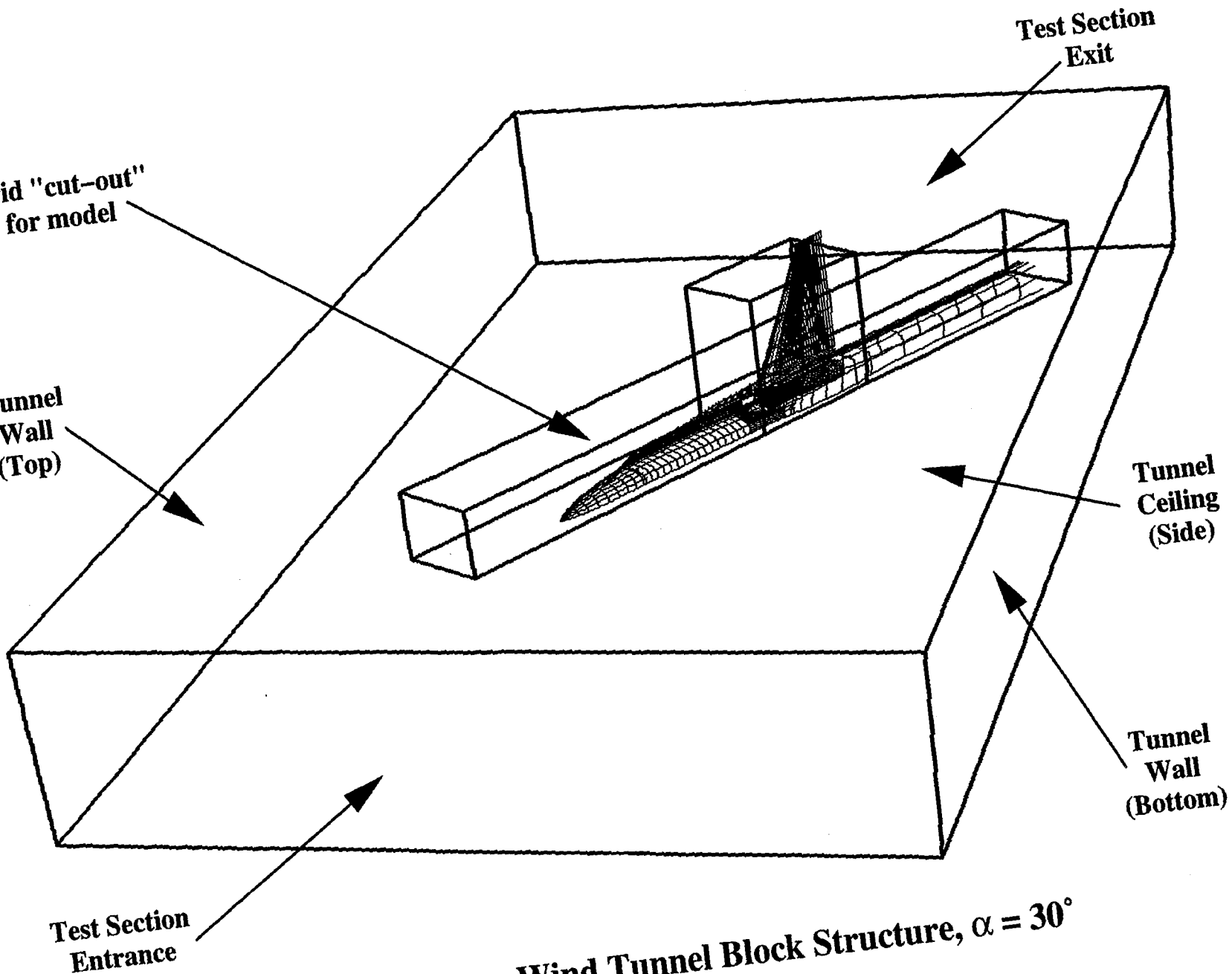

Fig. 4a – Wind Tunnel Block Structure, $\alpha = 30^{\circ}$

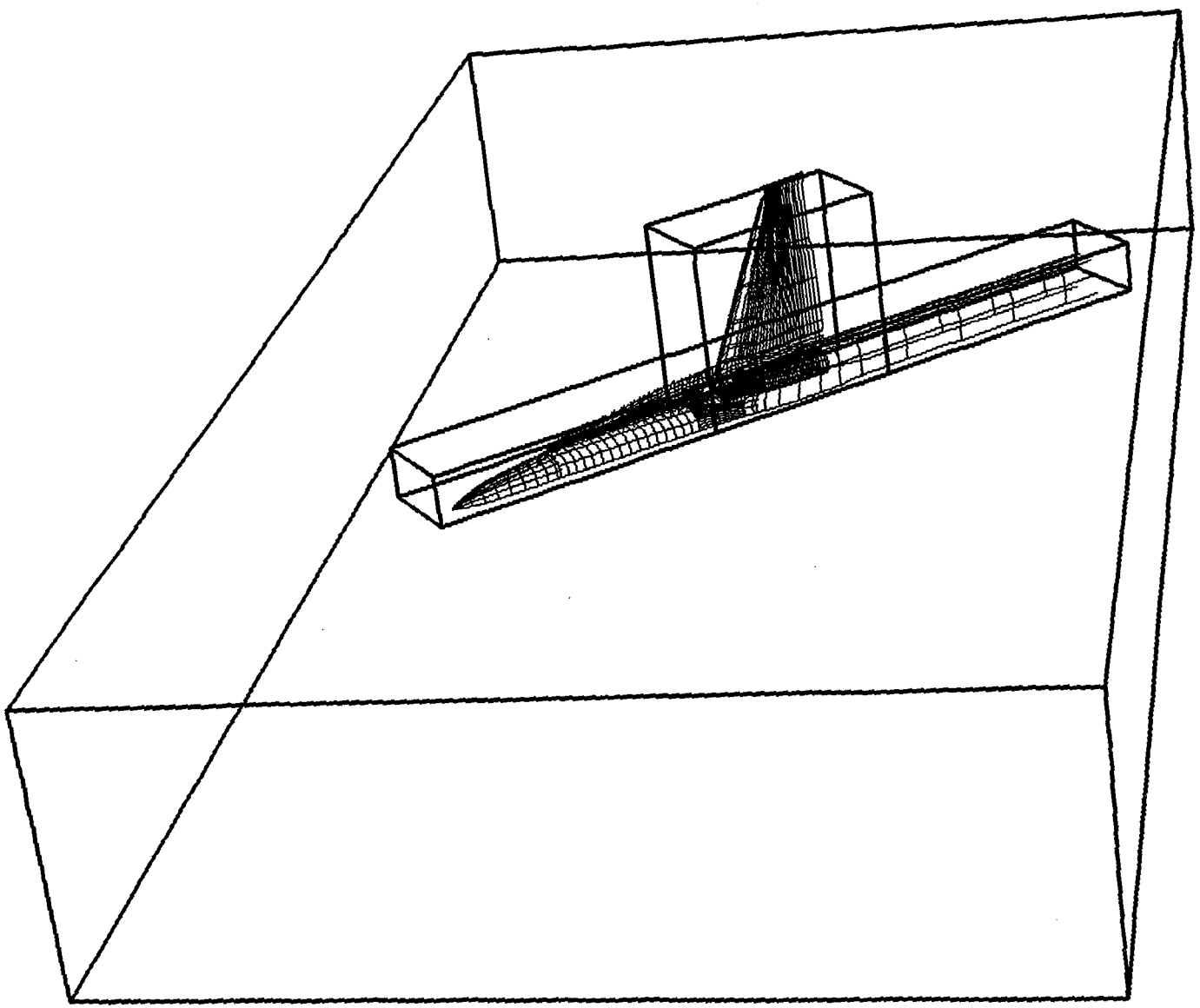

Fig. 4b – Wind Tunnel Block Structure, α = 50°

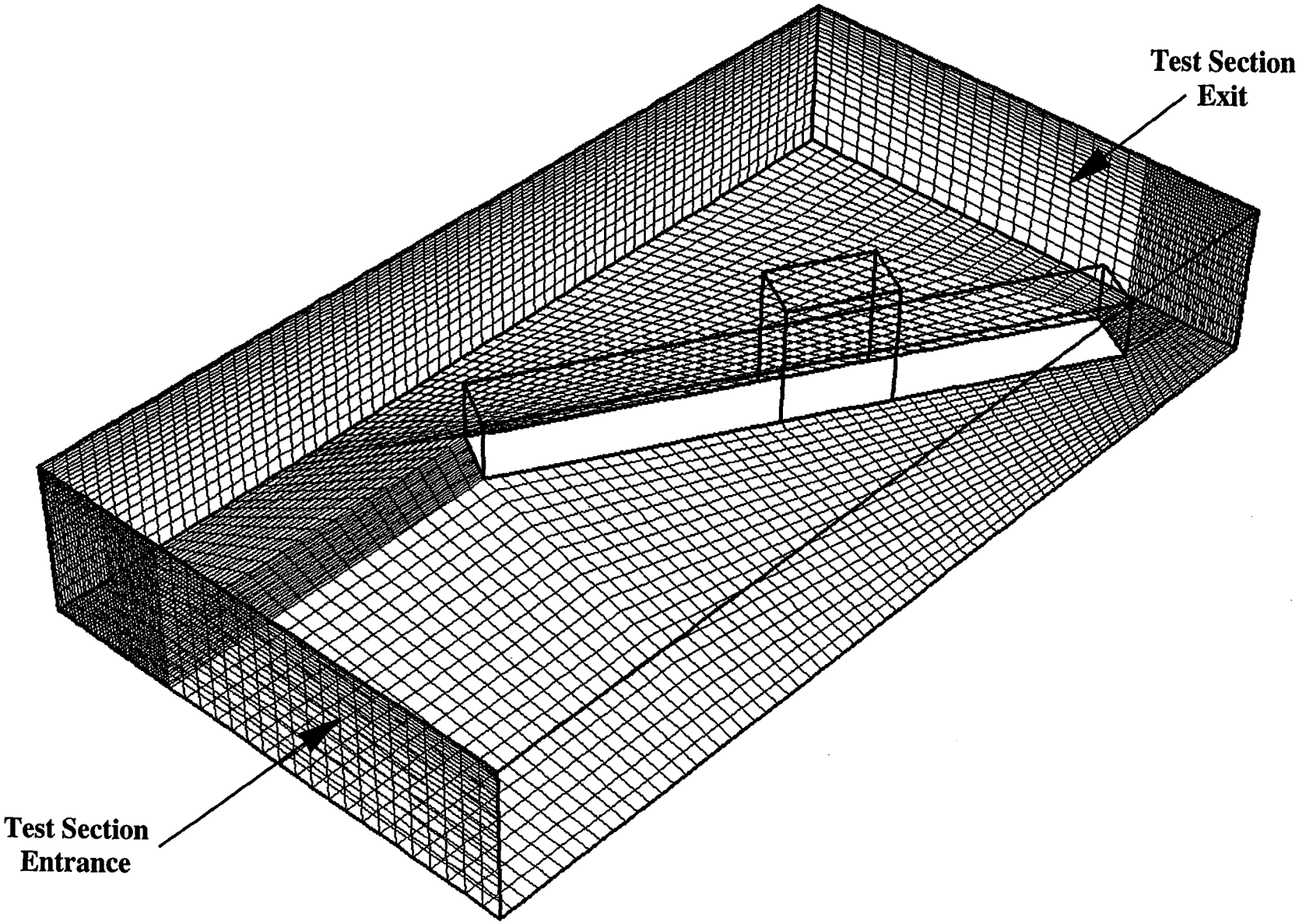

Fig. 5a – Wind Tunnel Surface Grid, $\alpha = 30°$

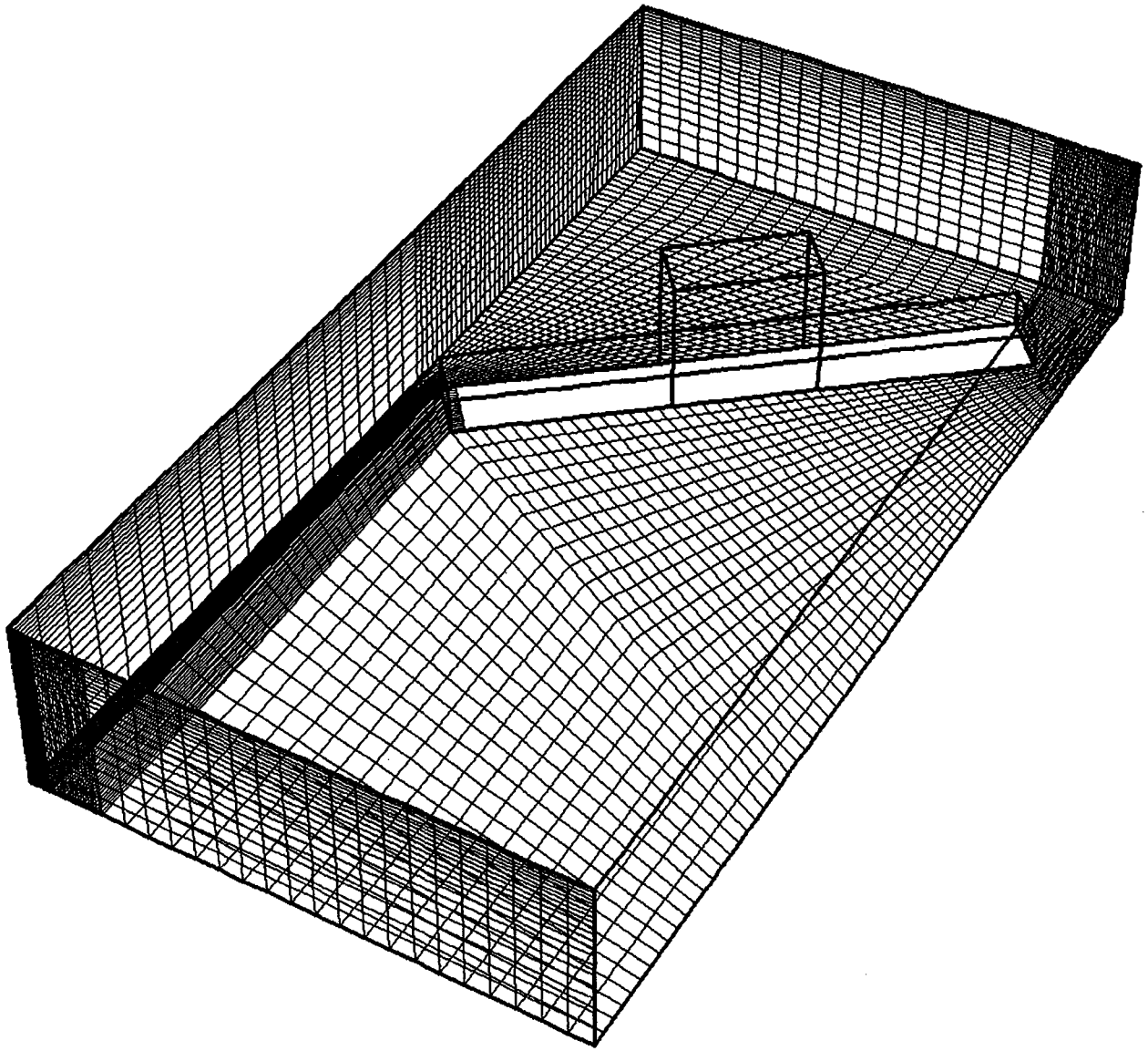

Fig. 5b – Wind Tunnel Surface Grid, $\alpha = 50^{\circ}$

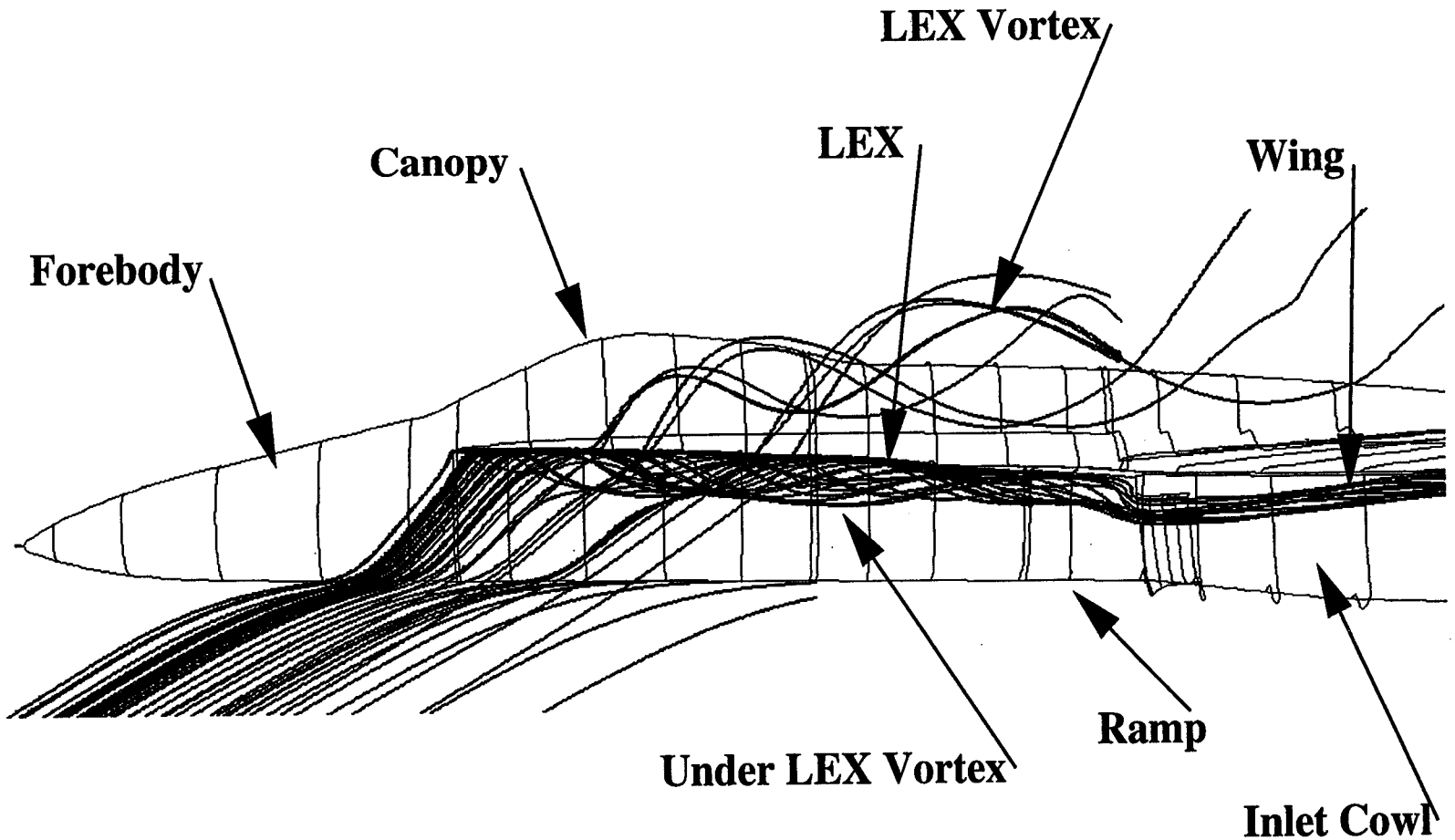

Fig. 6 – Typical Off–Body Particle Trajectories

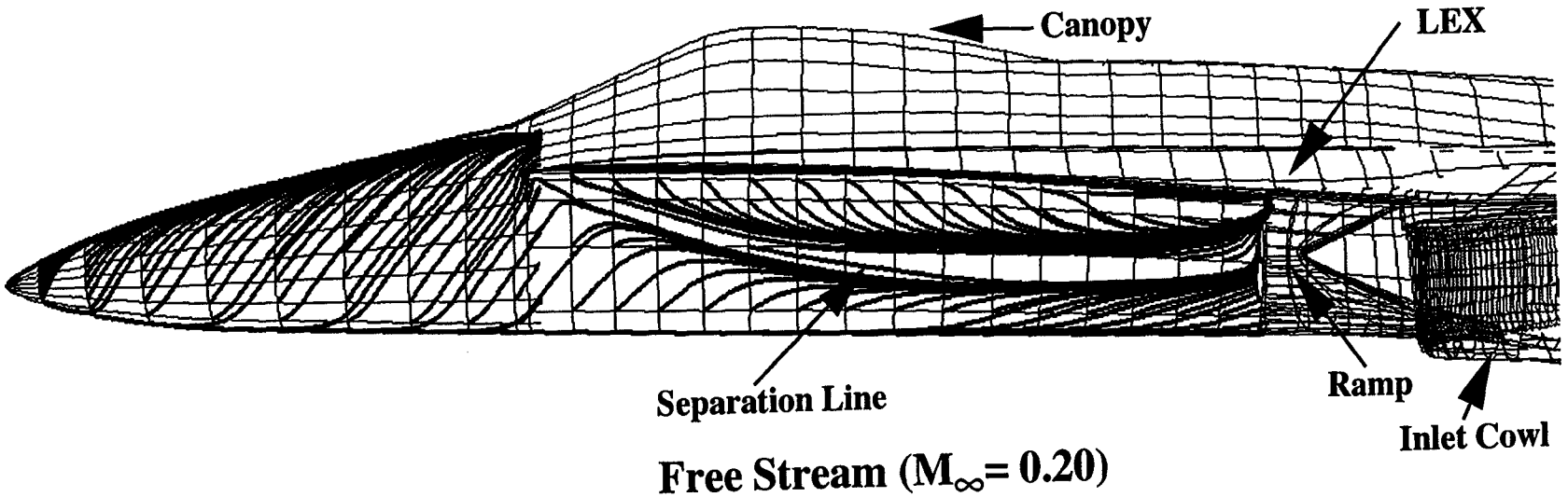

Free Stream (M_∞= 0.20)

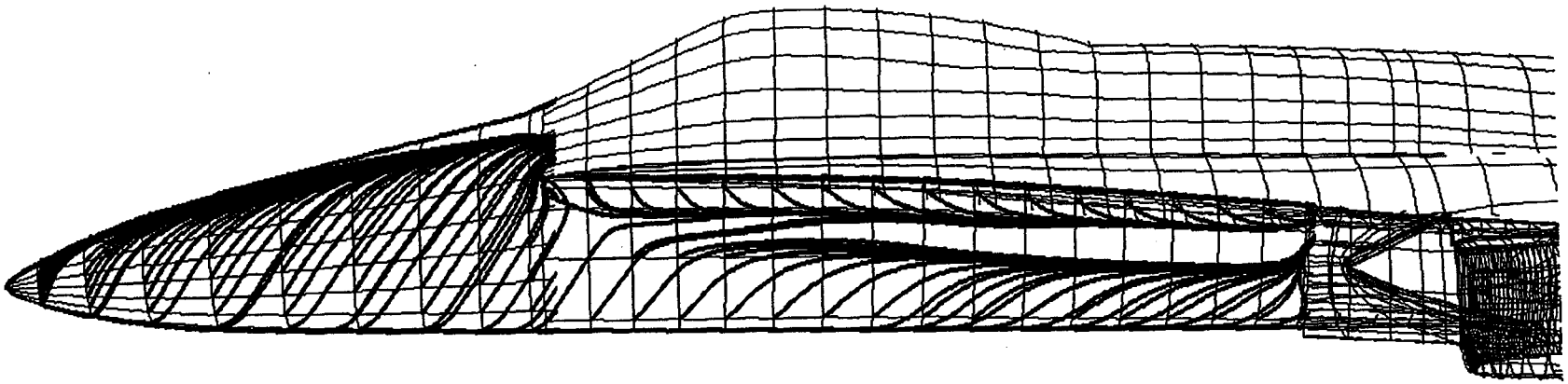

Wind Tunnel (M_∞ = 0.20)

Fig. 7a – Particle Trajectories Along Fuselage, 30° angle–of–attack

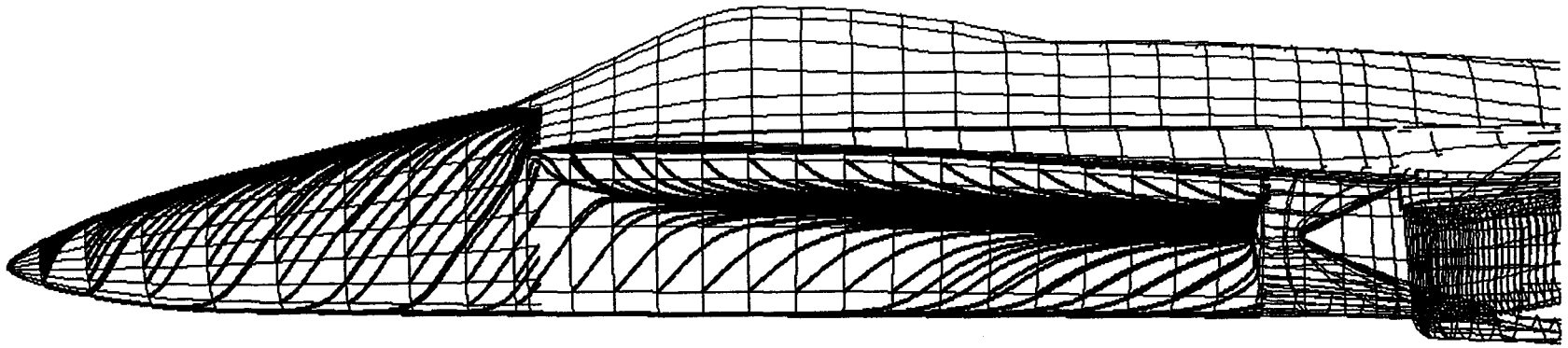

Free Stream ($M_\infty = 0.15$)

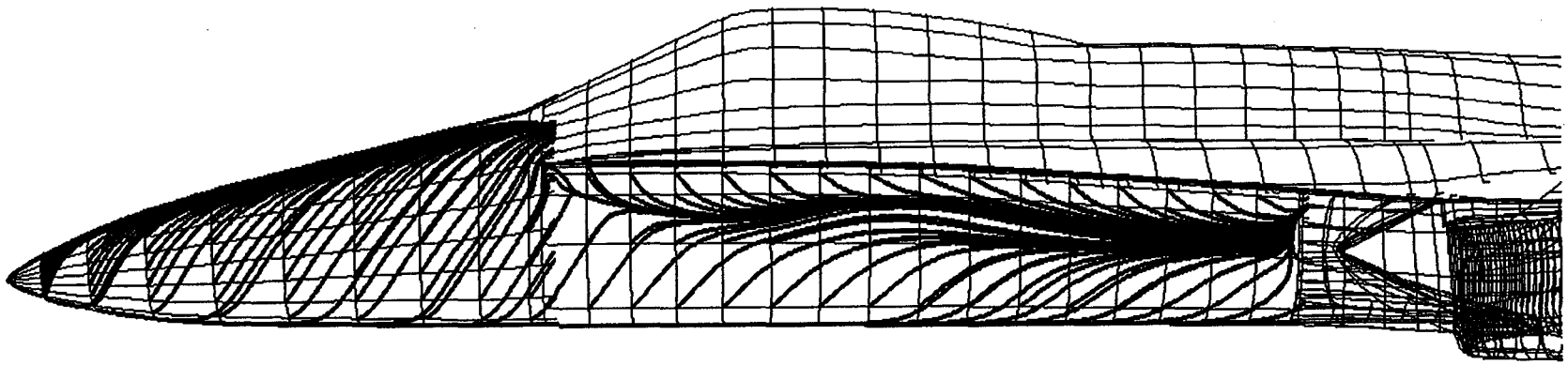

Wind Tunnel ($M_\infty = 0.15$)

Fig. 7a – Particle Trajectories Along Fuselage, 30° angle–of–attack (concluded)

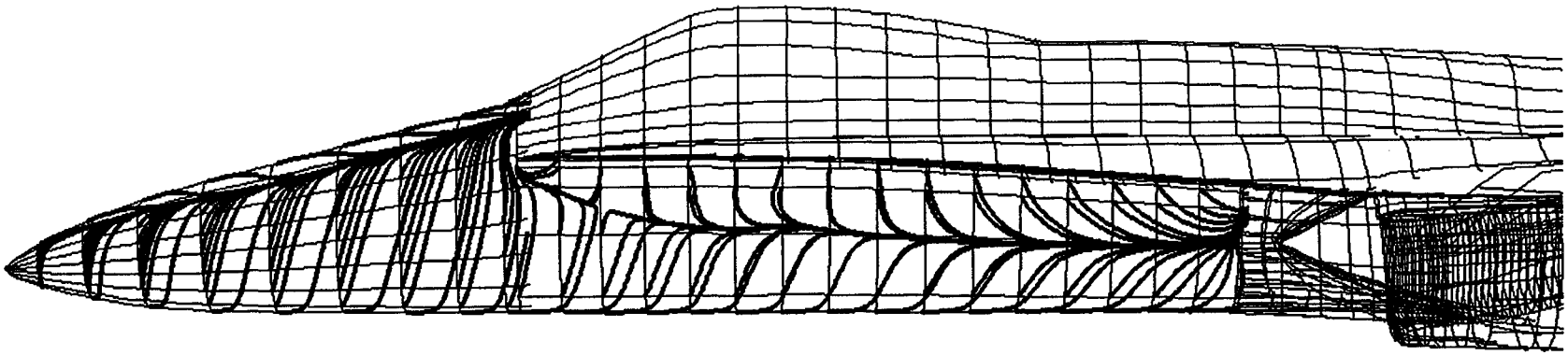

Free Stream ($M_\infty = 0.20$)

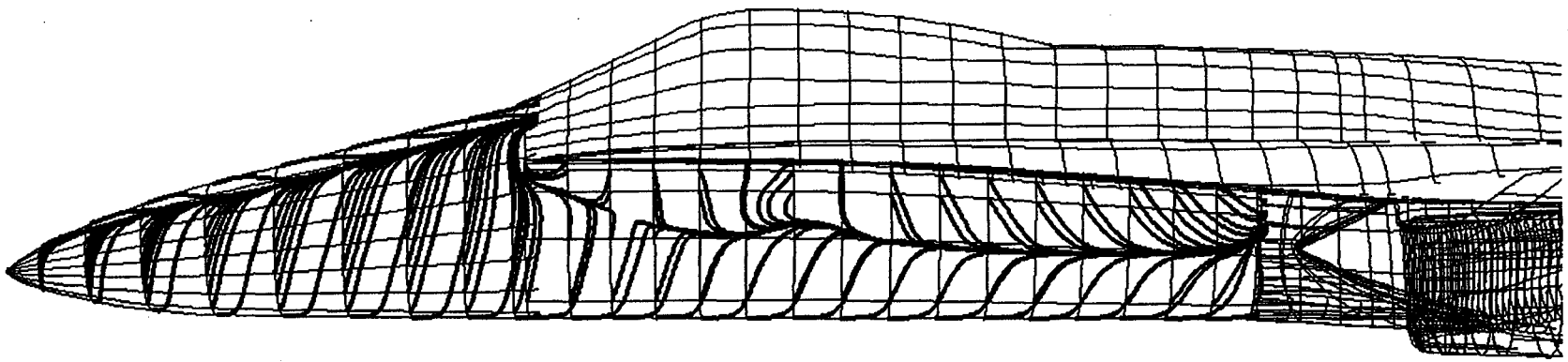

Wind Tunnel ($M_\infty = 0.20$)

Fig. 7b – Particle Trajectories Along Fuselage, 50° angle–of–attack

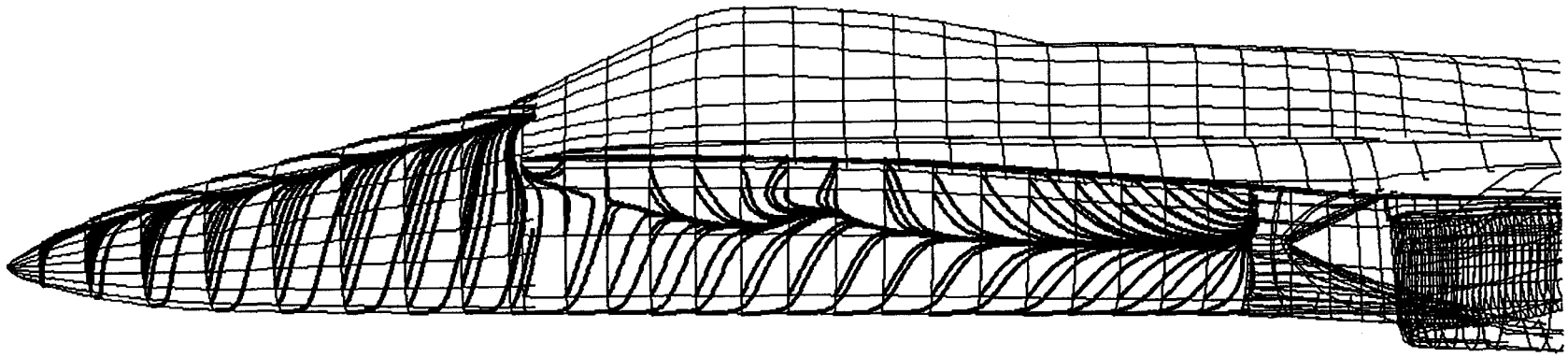

Free Stream ($M_\infty = 0.15$)

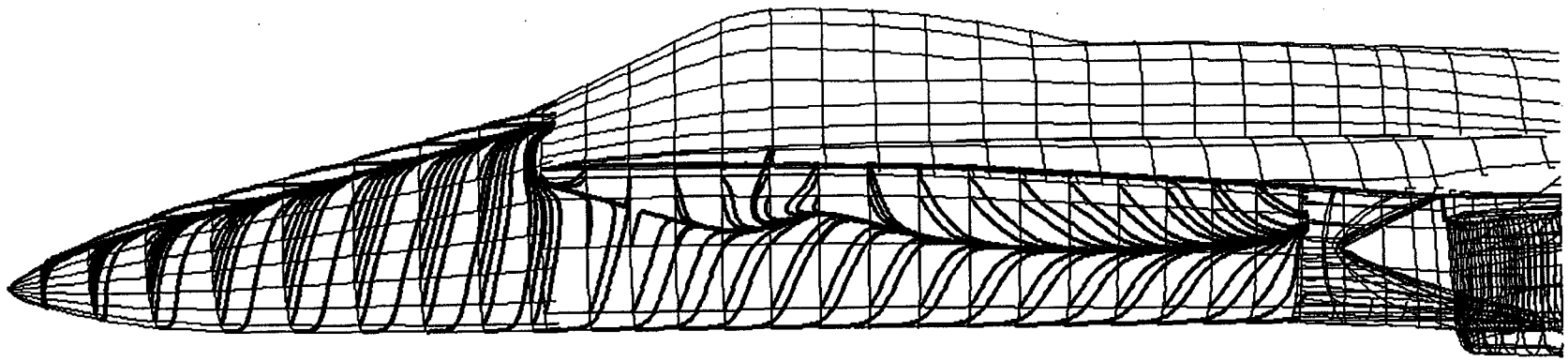

Wind Tunnel ($M_\infty = 0.15$)

Fig. 7b – Particle Trajectories Along Fuselage, 50° angle–of–attack (concluded)

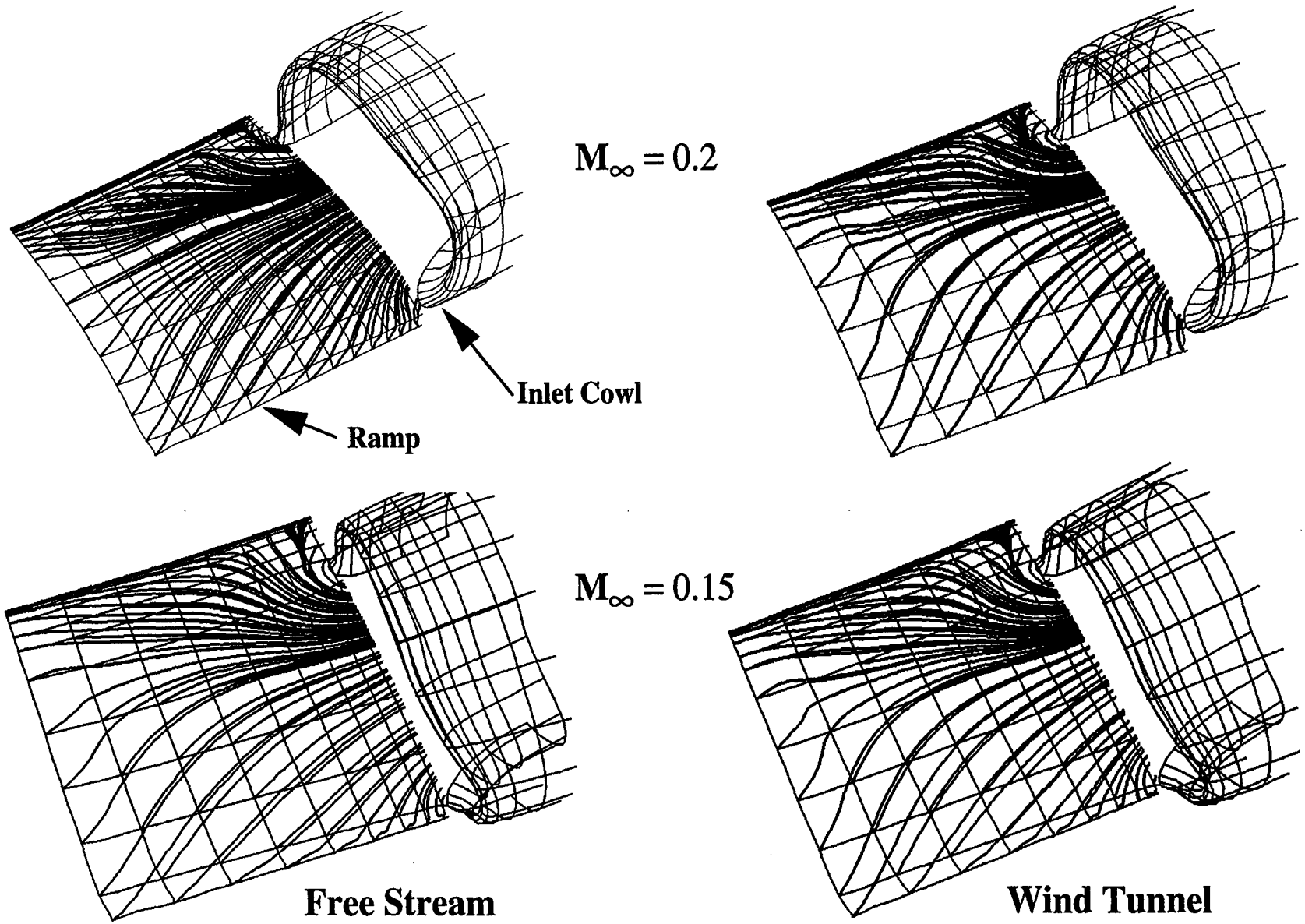

Fig. 8a – Particle Trajectories Along Ramp, 30° angle–of–attack

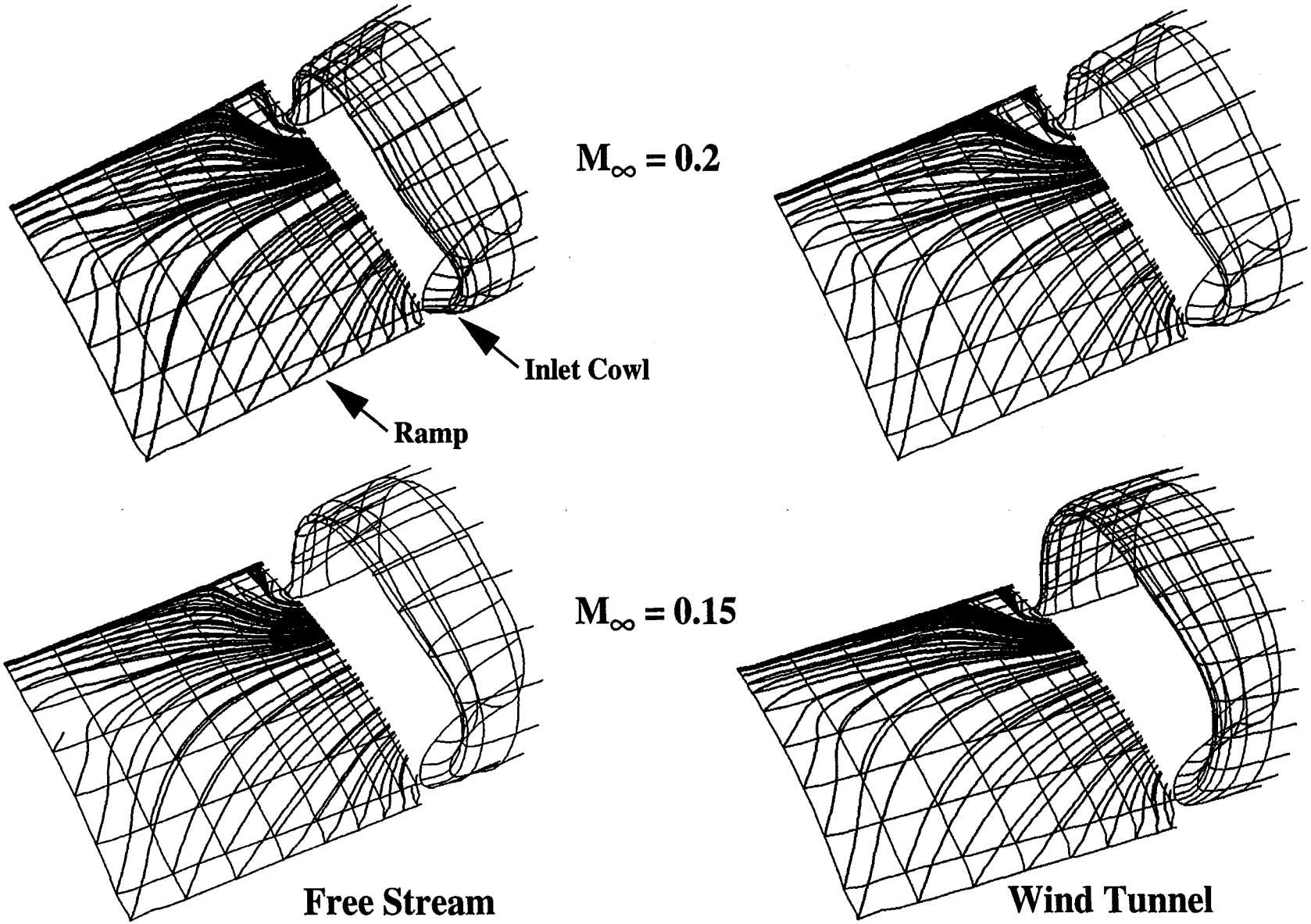

Fig. 8b – Particle Trajectories Along Ramp, 50° angle–of–attack

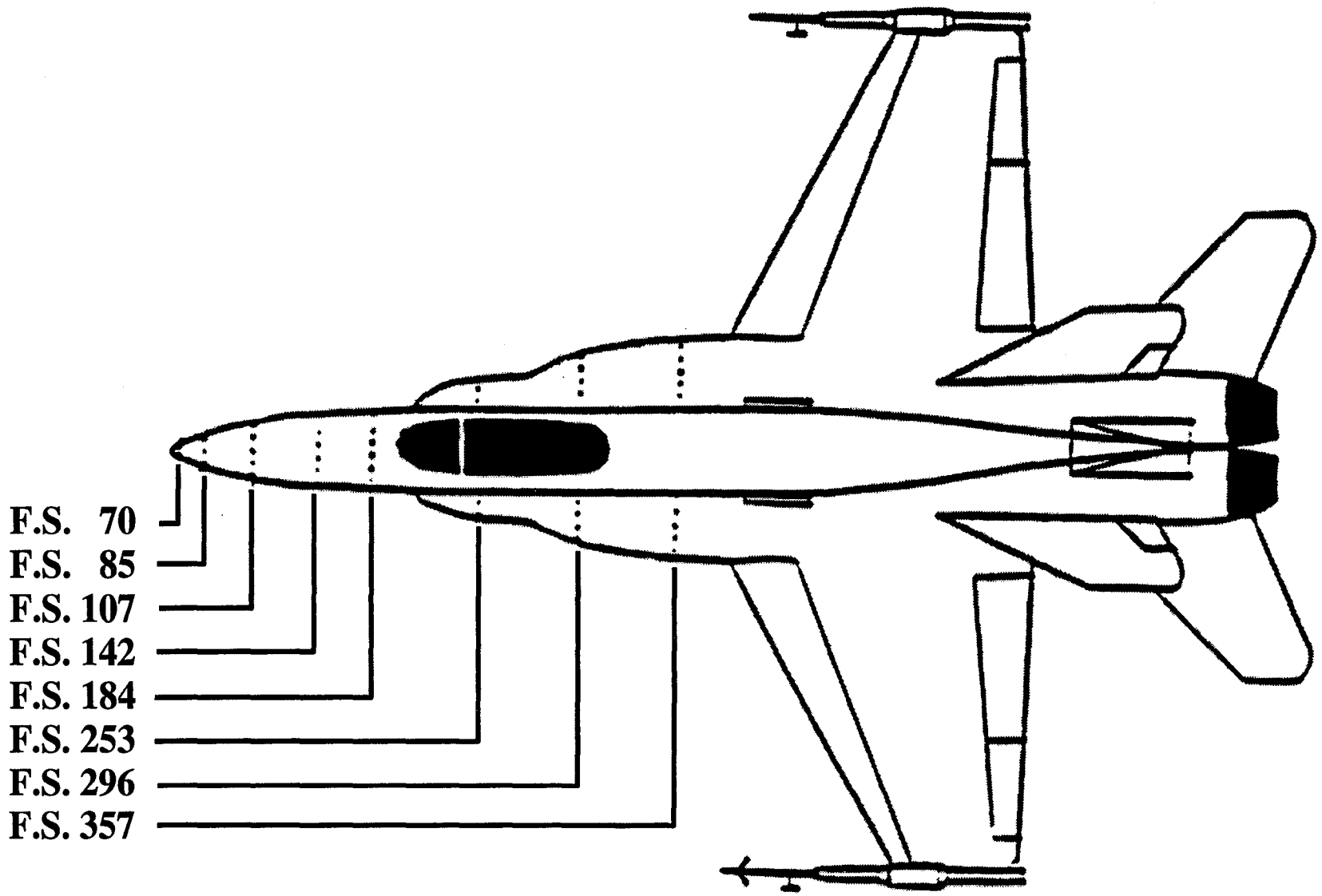

Fig. 9 – Forebody/LEX Surface Pressure Measurement Stations

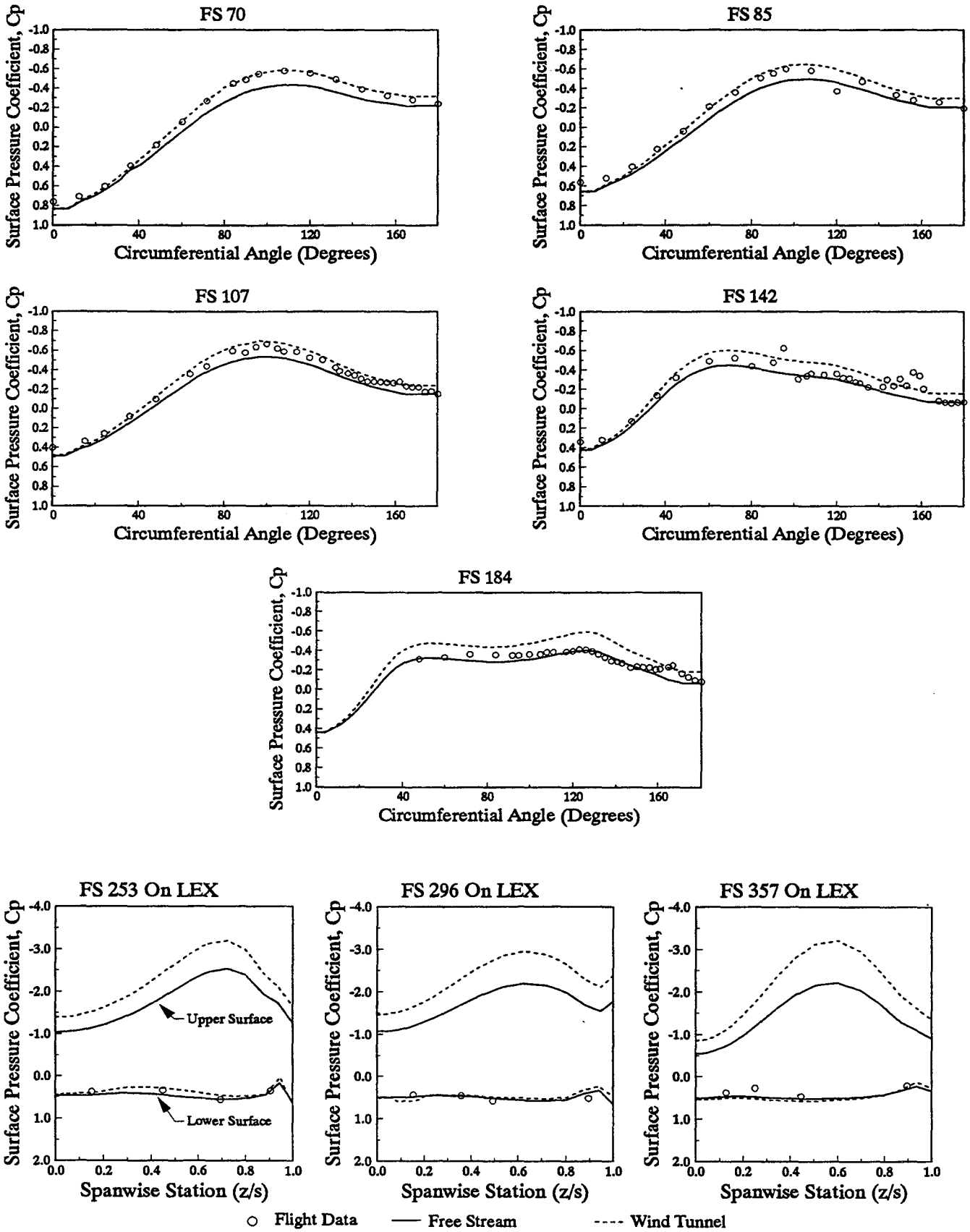

Fig. 10a - Forebody/LEX Surface Static Pressure Distributions, 30° angle-of-attack, M∞ = 0.20

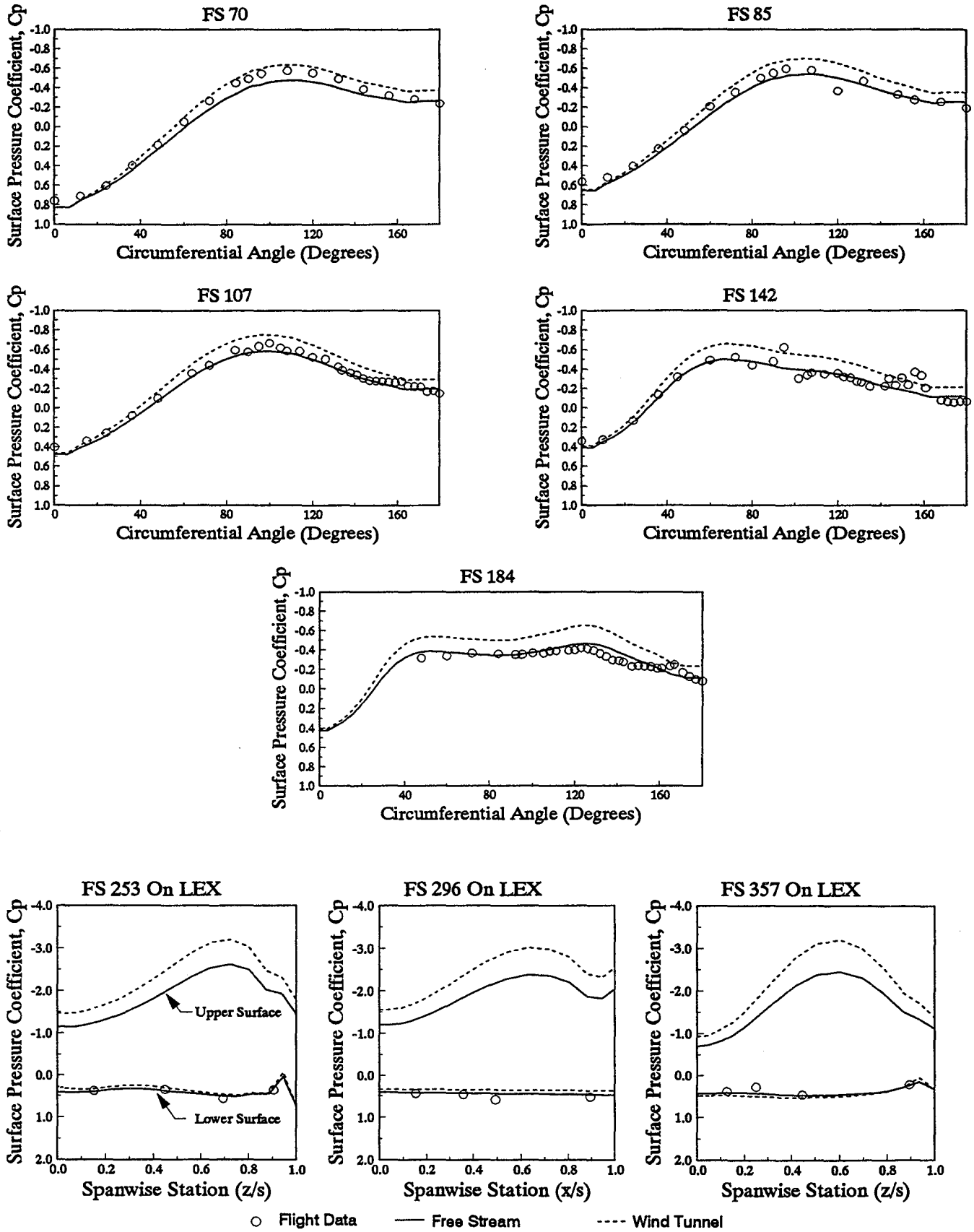

Fig. 10b - Forebody/LEX Surface Static Pressure Distributions, 30° angle-of-attack, M∞ = 0.15

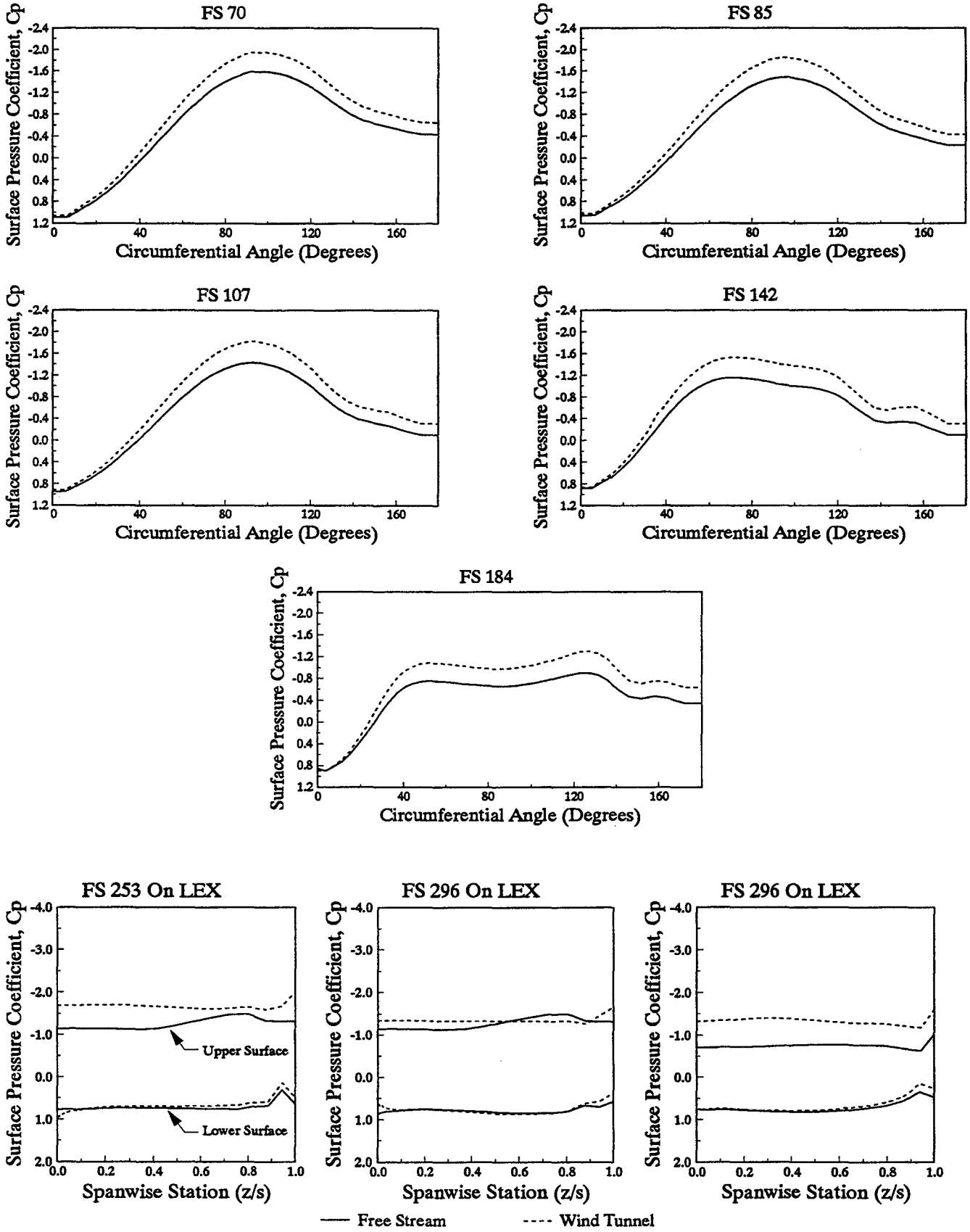

Fig. 10c - Forebody/LEX Surface Static Pressure Distributions, 50° angle-of-attack, M∞ = 0.20

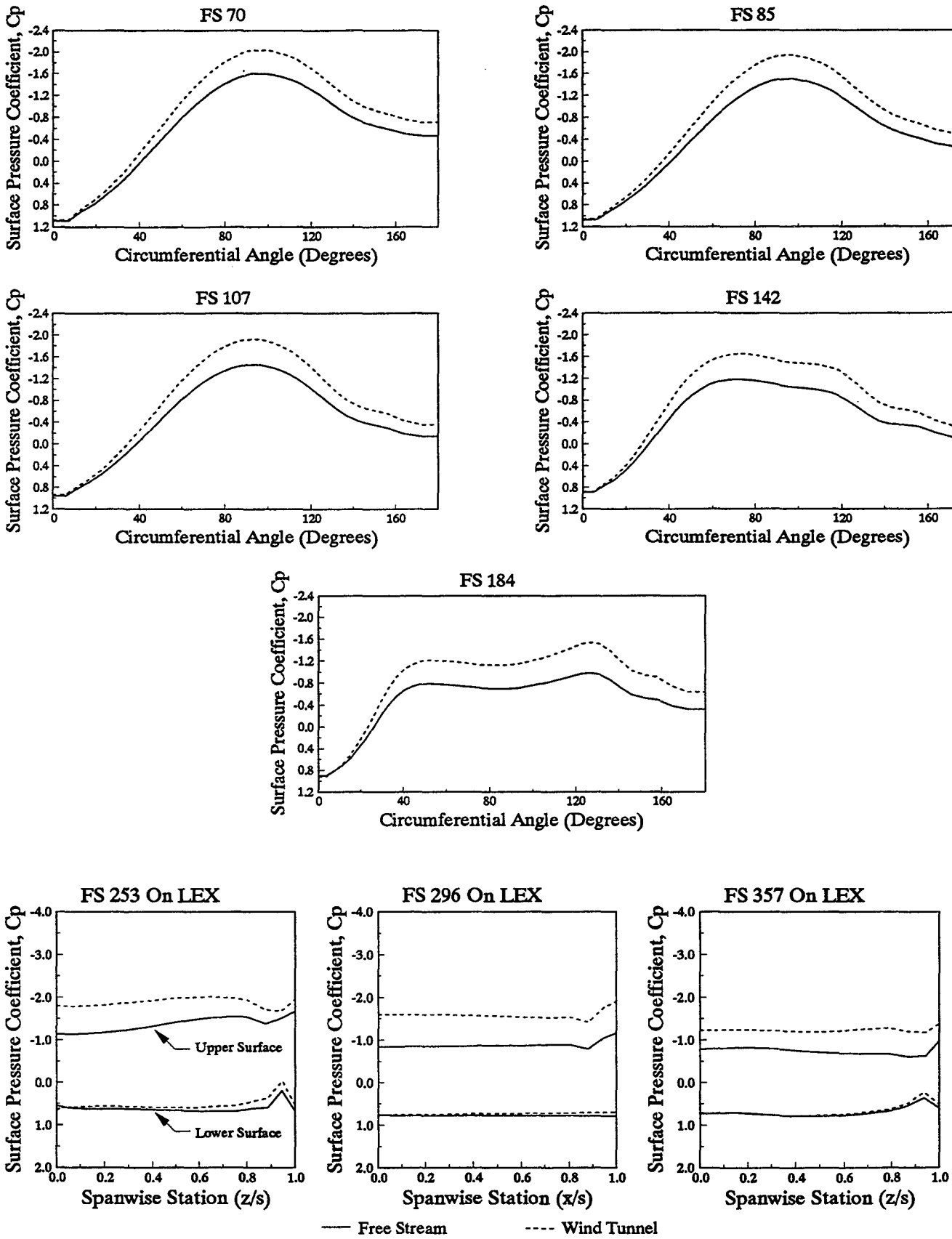

Fig. 10d - Forebody/LEX Surface Static Pressure Distributions, 50° angle-of-attack, M∞ = 0.15

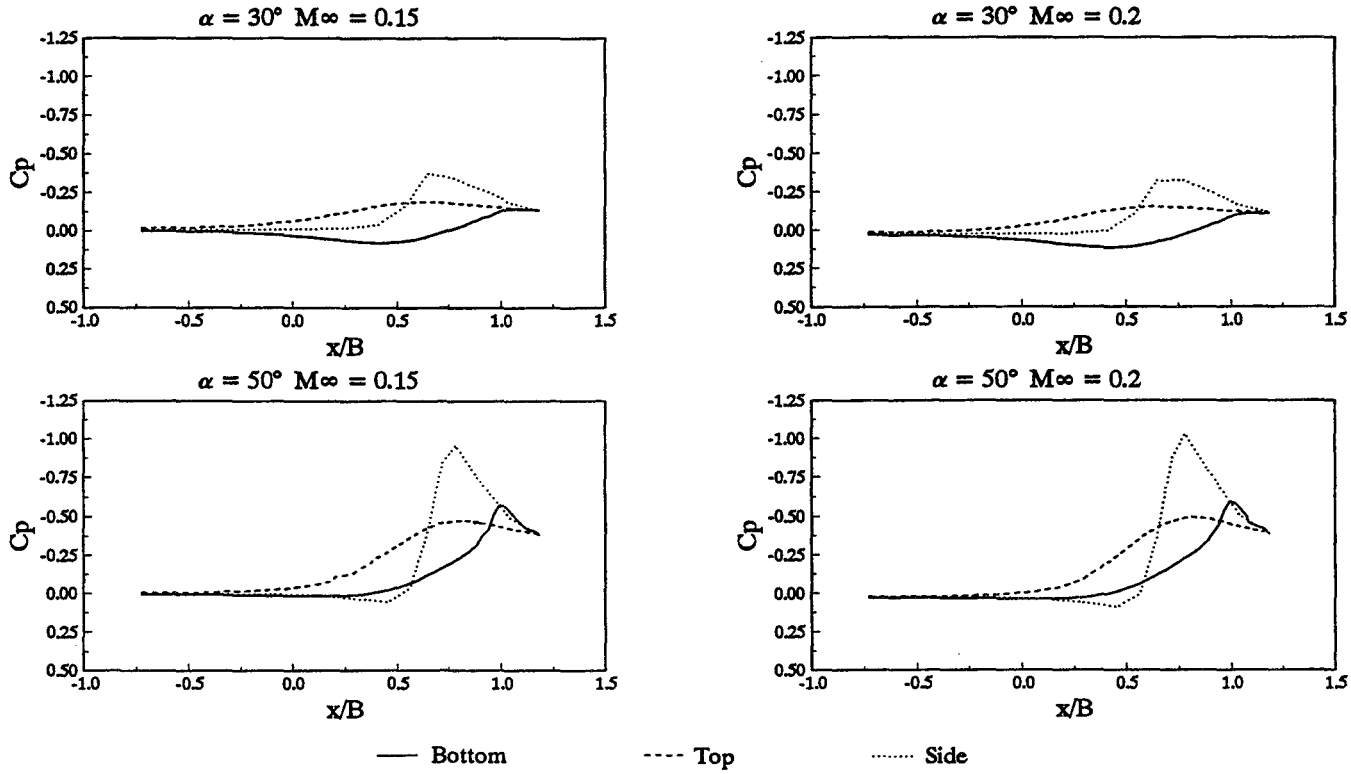

Fig. 11 - Wind Tunnel Static Pressure Coefficients

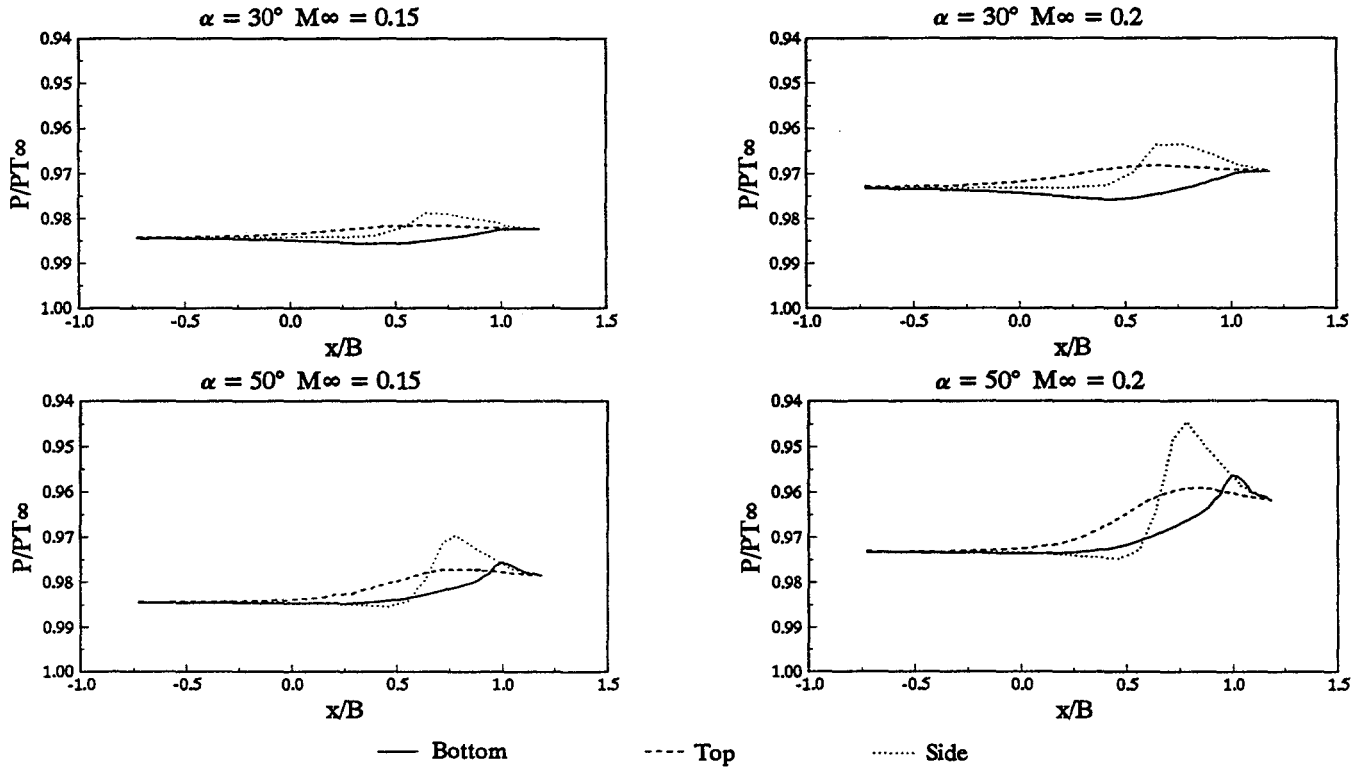

Fig. 12 - Wind Tunnel Wall Static-to-Total Pressure Ratios

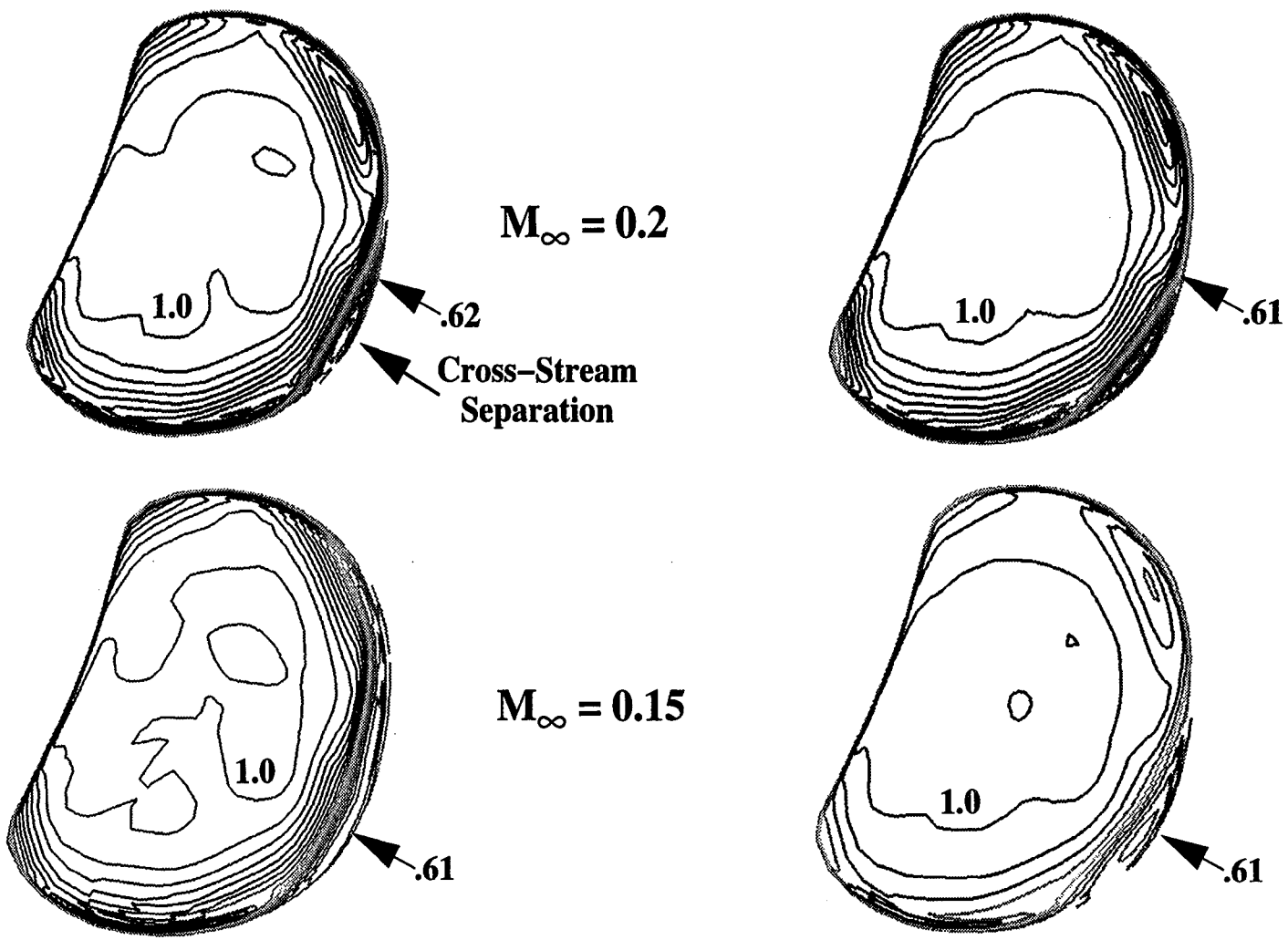

Fig. 13a – Inlet Entrance Total Pressure Contours (P_T/P_{T_∞}), 30° angle–of–attack

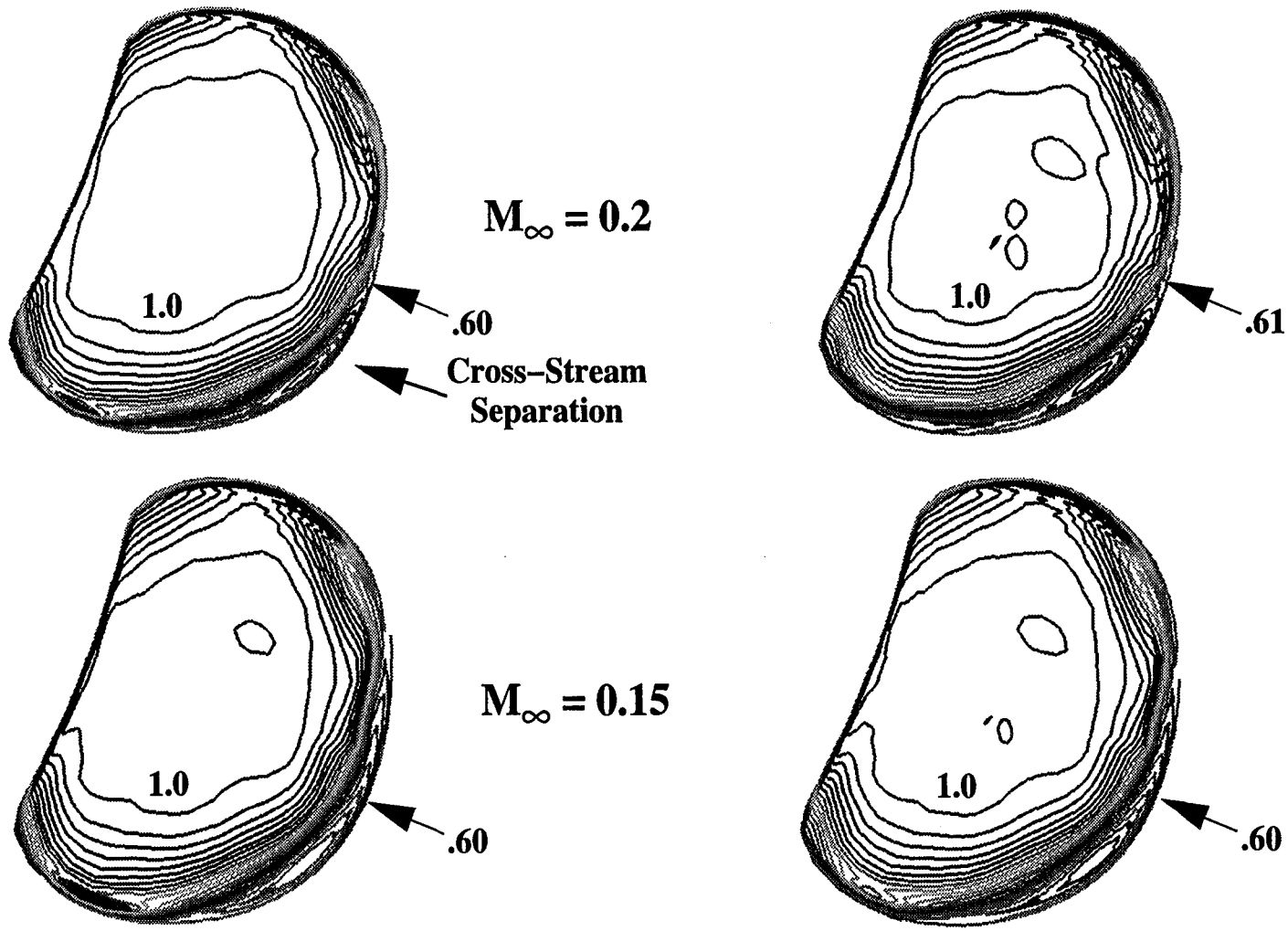

Fig. 13b – Inlet Entrance Total Pressure Contours (P_T/P_{T_∞}), 50° angle–of–attack

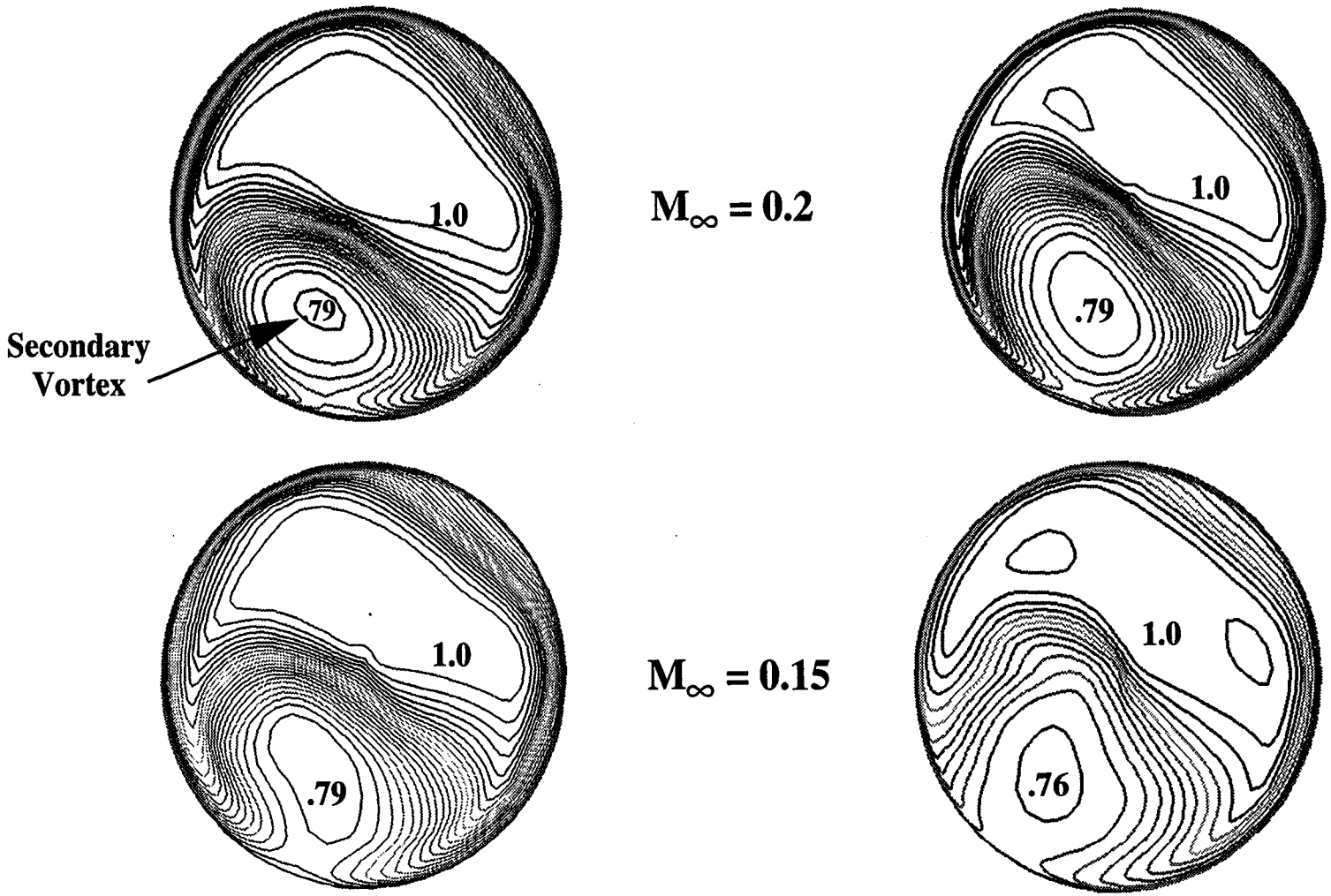

Fig. 14a – Compressor Face Total Pressure Contours (P_T/P_{T_∞}), 30° angle–of–attack

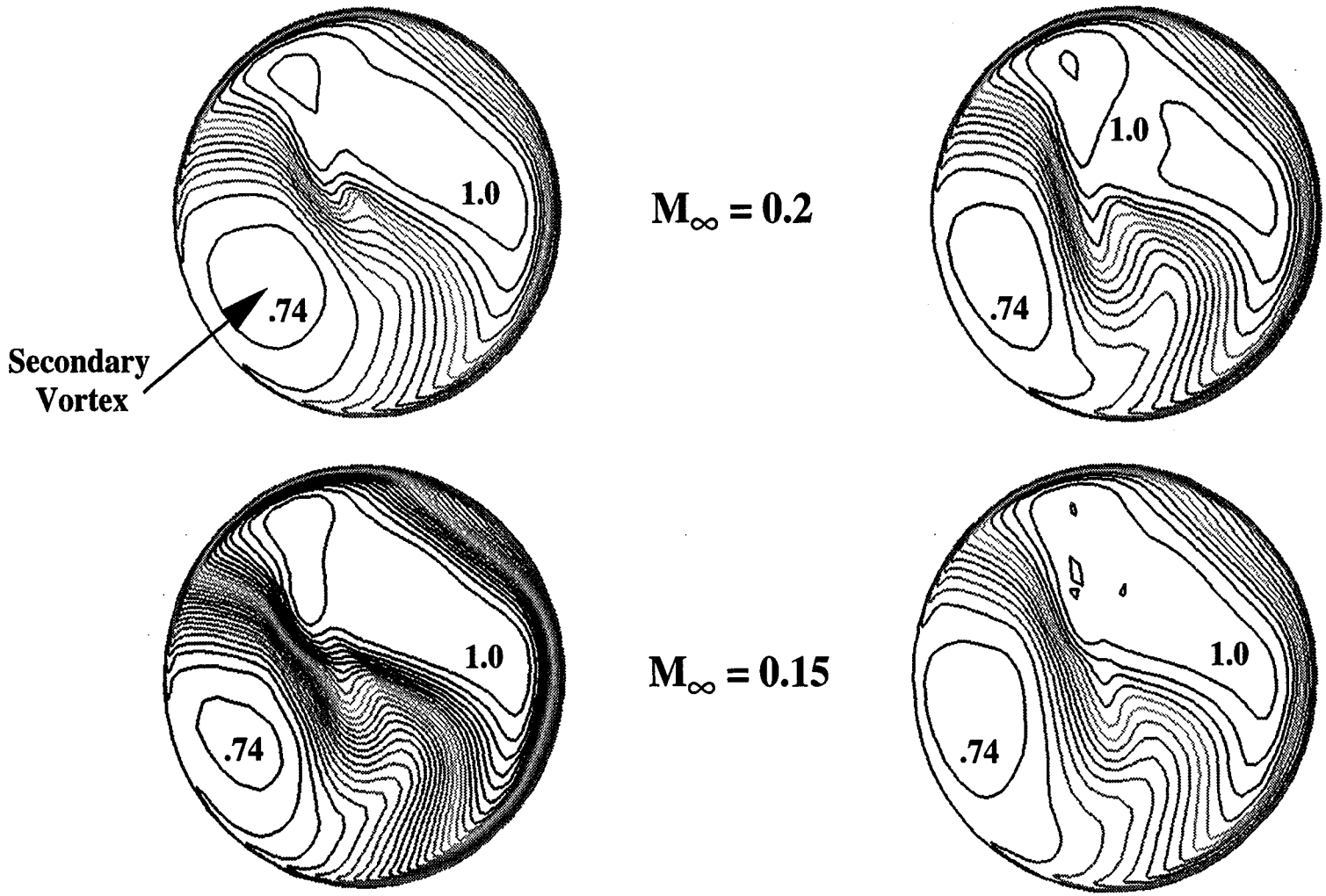

Fig. 14b – Compressor Face Total Pressure Contours (P_T/P_{T_∞}), 50° angle–of–attack

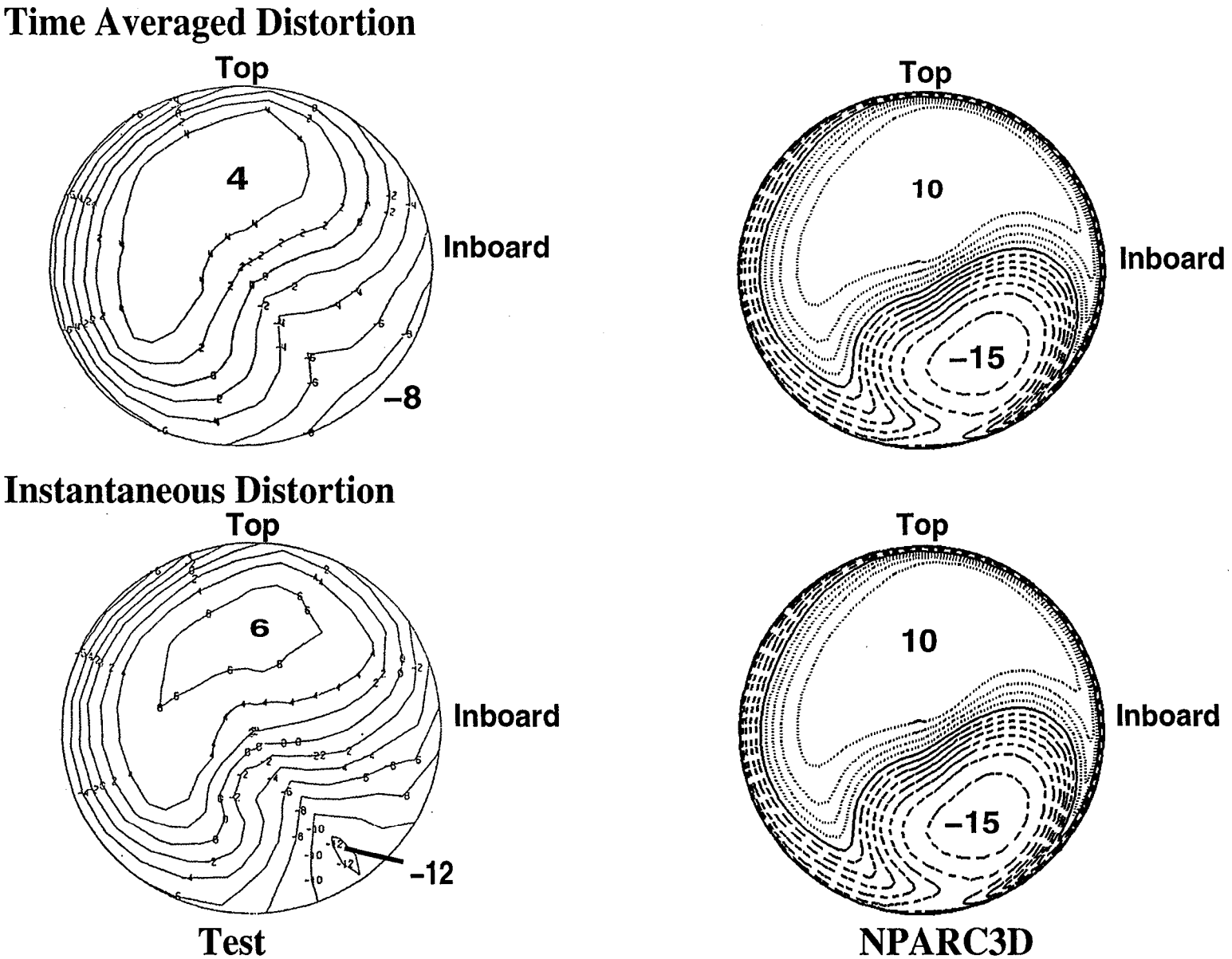

Fig. 15 – Wind Tunnel and Predicted Total Pressure Distortion Patterns $(P_T - P_{T_{avg}} / P_{T_{avg}})$

REPORT DOCUMENTATION PAGE

Form Approved
OMB No. 0704-0188

1. AGENCY USE ONLY (*Leave blank*)	2. REPORT DATE	3. REPORT TYPE AND DATES COVERED
	January 1995	Final Contractor Report

4. TITLE AND SUBTITLE

Prediction of Wind Tunnel Effects on the Installed F/A-18A Inlet Flow Field at High Angles-of-Attack

5. FUNDING NUMBERS

WU–505–68–30
C–NAS3–27186

6. AUTHOR(S)

Crawford F. Smith

7. PERFORMING ORGANIZATION NAME(S) AND ADDRESS(ES)

NYMA, Inc.
Engineering Services Division
2001 Aerospace Parkway
Brook Park, Ohio 44142

8. PERFORMING ORGANIZATION REPORT NUMBER

E–9416

9. SPONSORING/MONITORING AGENCY NAME(S) AND ADDRESS(ES)

National Aeronautics and Space Administration
Lewis Research Center
Cleveland, Ohio 44135–3191

10. SPONSORING/MONITORING AGENCY REPORT NUMBER

NASA CR–195429

11. SUPPLEMENTARY NOTES

Project Manager, Robert E. Coltrin, Propulsion Systems Division, NASA Lewis Research Center, organization code 2780, (216) 433–2181.

12a. DISTRIBUTION/AVAILABILITY STATEMENT

Unclassified - Unlimited
Subject Category 07

This publication is available from the NASA Center for Aerospace Information, (301) 621–0390.

12b. DISTRIBUTION CODE

13. ABSTRACT (*Maximum 200 words*)

NASA Lewis is currently engaged in a research effort as a team member of the High Alpha Technology Program (HATP) within NASA. This program utilizes a specially equipped F/A-18A, the High Alpha Research Vehicle (HARV), in an ambitious effort to improve the maneuverability of high-performance military aircraft at low-subsonic-speed, high angle-of-attack conditions. The overal objective of the Lewis effort is to develop inlet technology that will ensure efficient airflow delivery to the engine during these maneuvers. One part of the Lewis approach utilizes computational fluid dynamics codes to predict the installed performance of inlets for these highly maneuverable aircraft. Wind tunnel tests were a major component of the Lewis program. Since the available wind tunnel was small (9 x 15 ft) as compared to the scale of the model of the F/A-18A (19.78%), there were questions about the capability to obtain useful inlet performance data. The blockage effects were expected to be very large. This report represents the results of an analysis to determine how the wind tunnel walls affect inlet performance at several angles-of-attack. The predictions for the external particle traces along the fuselage indicate the influence of the wind tunnel side wall under the model is greater at 30° angle-of-attack than at 50° angle-of-attack on the under Leading Edge Extension (LEX) vortex trajectory. The side wall above the model appears to have negligible influence on the under LEX vortex. This may be due to the LEX acting as "shield" to the upper wall effects. As expected, the wind tunnel has a significant influence on the external forces. The lift and drag coefficients increase significantly for the wind tunnel model as compared to free stream conditions. The wind tunnel had a small effect on the inlet recovery and on inlet total pressure distortion patterns. The predicted recoveries for the wind tunnel model are within one percentage point of the model recoveries in free stream conditions.

14. SUBJECT TERMS

F/A-18; Wind tunnel; CFD; Flow calculation; High angle-of-attack

15. NUMBER OF PAGES

55

16. PRICE CODE

A04

17. SECURITY CLASSIFICATION OF REPORT	18. SECURITY CLASSIFICATION OF THIS PAGE	19. SECURITY CLASSIFICATION OF ABSTRACT	20. LIMITATION OF ABSTRACT
Unclassified	Unclassified	Unclassified	